

Hochschule für Angewandte Wissenschaften Hamburg Hamburg University of Applied Sciences

Masterarbeit

Jan Muller

Simulation of an Airborne Wind Energy System in the Atmosphere of Mars

Masterarbeit eingereicht im Rahmen der Masterprüfung

im Studiengang Fahrzeugbau bzw. Flugzeugbau am Department Fahrzeugtechnik und Flugzeugbau der Fakultät Technik und Informatik der Hochschule für Angewandte Wissenschaften Hamburg

Erstprüfer/in: Prof. Vera Schorbach Zweitprüfer/in: Prof. Peter Dalhoff

Abgabedatum: 05.12.2024

Zusammenfassung

Name des Studierenden

Jan Muller

Thema der Masterarbeit

Simulation einer Flugwindenergieanlage in der Atmosphäre des Mars

Stichworte

AWES, FlugwindenerWind Energie, Mars, Atmosphäre, Steuerung, Kite

Kurzzusammenfassung

Bisher basiert die Stromerzeugung bei Weltraummissionen häufig auf Solarpaneelen, die Sonnenenergie nutzen. Da jedoch der nächste Nachbar der Erde, der Mars, Staubstürme erlebt, die bis zu Monate andauern, verringert sich die Intensität der Sonnenstrahlung auf der Marsoberfläche erheblich (Schorbach und Weiland, 2022). Der Energiebedarf einer bemannten Mission zum Roten Planeten kann daher nicht allein auf Solarenergie basieren. Daher wird der Einsatz eines luftgestützten Windenergiesystems in Betracht gezogen, das die allgemein Windgeschwindigkeiten der Marsatmosphäre nutzt. Während der theoretische Einsatz eines solchen Systems bereits diskutiert wurde, wurde eine Simulation der Flugbahn eines Drachens unter den atmosphärischen Bedingungen des Mars noch nicht vorgestellt. Durch die Untersuchung der Windbedingungen an potenziellen Landeplätzen für zukünftige bemannte Missionen mithilfe der Martian Climate Database (MCD) (F. Forget, E. Millour, T. Pierron, M. Vals and V. Zakharov (LMD), and the MCD team) werden die Windgeschwindigkeit und die atmosphärische Dichte für einen Anwendungsfall ermittelt. In dieser Arbeit werden die Abmessungen eines Referenz-Kites mithilfe 2024 einer von Gaunaa et al., abgeleiteten Skalierungsmethode an die Atmosphäre des Mars angepasst. Der skalierte Kite wird dann in LAKSA, einem Lagrange-Drachensimulator, implementiert, um eine potenzielle Flugbahn für die Leistungserzeugung zu analysieren. Mit Hilfe einer simulierten Flugbahn, die nicht für eine repräsentative Ausrollphase geeignet ist, wird die theoretische Leistungsabgabe des Kites berechnet.

Title of the paper

Simulation of an Airborne Wind Energy System in the Atmosphere of Mars

Keywords

AWES, wind power, Mars, atmosphere, control

Abstract

So far, power generation of space missions has always been based on solar panels harnessing solar energy. However, Earth's closest neighbour Mars, is located further from the sun than Earth and experiences dust storms lasting up to months, resulting in a significantly reduced intensity of solar radiation on the Martian surface (Schorbach and Weiland, 2022). Thus, energy requirements of a manned mission to the Red Planet cannot solely be based on solar energy. Therefore, the use of an airborne wind energy system is considered, utilising the generally higher wind speeds the Martian atmosphere exhibits. While the theoretical deployment of such a system has already been discussed (Schmehl et al., 2024; Gaunaa et al., 2024), a simulation of a flight path in the Martian atmospheric conditions has not been presented yet. By investigating the wind conditions at potential landing sites for future manned-missions using the Martian Climate Database (MCD), the wind speed and atmospheric density for a use-case are derived (A. Spiga (LMD) and Web interface updated by T. Pierron (LMD) and A. Bierjon (LMD)). In this thesis the dimensions of a reference kite are adjusted to the atmosphere of Mars utilizing a scaling method derived from (Gaunaa et al., 2024). The scaled kite is then implemented into LAKSA, a Lagrangian Kite Simulator, to analyse a potential figure-of-eight generated for the reeling out during power generation. With a trajectory simulated that is not suitable for a representative reel-out phase, the theoretical power output of the kite is calculated.

Table of Figures

Figure 1:	Comparison of rotor area of the tips of conventional wind turbines and the flight path of different AWES concepts with respect to power generation and structure
Figure 2:	Distinction of AWESs concerning the position of the generator; (a) Ground-Generation; (b) Fly-Generation
Figure 3:	Pumping Cycle; (a) reel-out/generation phase; (b) reel-in/recovery phase13
Figure 4:	Kite concepts utilising on-board electricity generation; (a) plane with turbines; (b) airframe with wings and turbines; (c) Aerostatic balloon with centre turbine; (d) autorotational quadcopter
Figure 5:	Several rigid and soft kite designs for Ground Generation; (a-c) soft and flexible kite designs; (d, e) rigid wing designs; (f) semi-rigid wing 16
Figure 6:	methods for kite control; a) deflectors on-board; b) control unit for bridle lines; c and d) usage of power and control lines
Figure 7:	Real (blue line) and idealised (dashed line) flight path during a pumping cycle with the elevation angles during reeling
Figure 8:	colourised topography of the Martian surface including landing sites of Martian lander missions
Figure 9:	solar longitudes of the martian orbit with exaggerated eccentricity; colorization according to day-time surface temperature ranging from 40K (deep purple) to 315K (bright red)
Figure 10:	Example of the impact of a GDS in 201826
Figure 11:	Grid structure of a GCM spanning the Martian surface and atmosphere
Figure 12:	Frames of Reference used in LAKSA; (a) Body frame of reference of the kite with respect to the Earth Frame of Reference with wind speed W_0 ; (b) kite and arrangement of Bridle Lines; (c) orientation of bridle line with respect to the bridle length I, the bridle angles δ and η
Figure 13:	Marked locations as potential landing Spots for a manned Mars mission
Figure 14:	Atmospheric density at 35.23N 163.95E in 250m as simulated by the MCD

Figure 15:	Horizontal wind speeds at 35.23N 163.95E in 250m as simulated by the MCD41
Figure 16:	Simulation results of reference kite using the periodic orbit solver; (a) trajectory in XYZ-coordinate system; (b) velocities in their respective coordinate; (c) error with respect to classical mechanics; (d) top to bottom: length of tether rods, bridle line length, bridle angle δ , change of bridle line angle η during manoeuvre
Figure 17:	Simulation results of the scales Mars kite not using the periodic orbit solver; (a) trajectory in XYZ-coordinate system; (b) velocities in their respective coordinate; (c) error with respect to classical mechanics; (d) top to bottom: length of tether rods, bridle line length, bridle angle δ , change of bridle line angle η during manoeuvre
Figure 18:	long term behaviour of Mars kite with periodic fluctuations 47
Figure 19:	simulated tether forces of the reference kite (purple) and the scaled Mars kite (blue)
Figure 20:	Comparison of angle of attack α and the side slip angle β of the reference trajectory utilising the periodic orbit solver (blue) and the Mars kite trajectory without the periodic orbit solver (orange)

Table of Tables

Table 1: LAKSA kite parameters and scaling factors	43
Table 2: Control input of reference kite using Periodic orbit solver	44
Table 3: Control input of the scaled Mars kite	47
Table 4: Input parameters for power calculation	50

Table of Contents

Tal	ole of	Figu	ıres	5	
Tal	ole of	Tabl	les	7	
1	Intro	oduct	tion	9	
2	Lite	ratur	e Review	10	
2	2.1	Airb	orne Wind Energy	10	
	2.1.	1	Classification	11	
	2.1.	2	Wind Energy and Power	18	
2	2.2	Mar	·s	23	
	2.2.	1	The Martian Atmosphere	24	
	2.2.	2	Wind Energy on Mars	26	
2	2.3	Sim	ulations	31	
	2.3.	1	Martian Climate Database (MCD)	31	
	2.3.	2	LAKSA	33	
3	Met	hodo	ology	37	
4	Res	ults .		40	
4	.1	Win	d Field Analysis	40	
4	.2	LAK	(SA Simulation	43	
4	.3	The	oretical Power Output	50	
5	Discussion				
6	Conclusion54				
7	Deferences				

1 Introduction

As the closest planet to Earth Mars is logically humanity's first interplanetary destination. With the technology of propulsion rapidly succeeding, the research interest for organizing sustainable human missions is increasing. Next to a thin and oxygen poor atmosphere, no known liquid water reserves as well as a deserted and rocky landscape, the planet's climate brings further challenges such as extreme temperatures and dust storms that can last for weeks and months. Furthermore, the use of solar panels as the usual means to generate power for space missions faces difficulties with an overall lower solar radiation intensity due to distance and blocking by sand and dust. While the afore mentioned dust storms deny the continuous harnessing of solar radiation as a stable source of energy, the solar energy yield is generally lower than on Earth due to the increased distance from the sun. Therefore, finding a reliable energy source in all weather conditions on the red planet is a key factor for achieving a successful manned mission to our planetary neighbour. Airborne wind energy systems promise a high energy density and simultaneously indicate a steady energy delivery by harnessing the energy of unobstructed winds over 100 m above the surface - on paper.

This thesis aims to verify the applicability of airborne wind energy systems in the Martian atmosphere by simulating a possible trajectory using data from a climate model. After a short introduction to airborne wind energy in general, Mars as well as its atmosphere are described. Following a chapter, introducing the utilised simulation tools, the general approach to answer the research question are presented. With the results and an in-depth discussion thereof, this work will end with an overview of possible research topics in the future.

2 Literature Review

Before discussing the research question this chapter aims to introduce the fundamentals and enable a broader understanding of the topic. This includes presenting the developments in the Airborne Wind Energy sector, the underlying mechanics as well as the basics of the Martian atmospheric dynamics. First, an introduction to the field of Airborne Wind Energy Systems (AWES) is given, as well as a technological and mathematical description of the sector at the time of writing. It is followed by a chapter dedicated to Mars, its atmospheric conditions and phenomena, and the state of research concerning wind energy on Mars. Finally, the software involved in this work including the atmospheric modelling and simulation tool utilised for the research questions are described.

2.1 Airborne Wind Energy

In 1980 the American engineer Miles Loyd introduced the concept of Airborne Wind Energy Systems or AWES to the scientific community with his publication of "Crosswind Kite Power". In his paper Miles Loyd describes the extraction of wind energy using kites, which he defined as "aerodynamic vehicle[s] restrained by a tether". With kites, the size of military transport aircrafts he envisioned systems with the ability to generate power several tens of megawatts (Loyd, 1980).

In contrast to conventional wind turbines, these kite systems are to be deployed at altitudes of several 100 m making it possible to harness the energy of high-altitude-winds (Cherubini *et al.*, 2015; Loyd, 1980; Diehl *et al.*, 2013). At these altitudes, winds are no longer affected by the frictional forces induced by the flow of air over the surface of the Earth. As fluids, in this case air, flows along a surface, frictional effects lead to the formation of a boundary layer, in which the airflows speed is reduced, and turbulence is induced. The height of the Earth's boundary layer varies between around 100m over the open sea to up to 1 km over terrain (Peng *et al.*, 2023; Bechtle *et al.*, 2019). Outside of the boundary layer air flow or wind speeds are higher and unidirectional due to its laminar, non-turbulent, flow characteristics, thus significantly increasing its kinetic energy. The use of these continuous high-velocity air flows by deploying airborne devices in heights of up to 1000 m promises the potential for high energy yields (Cherubini *et al.*, 2015; Bechtle *et al.*, 2019; Khan and Rehan, 2016).

Compared to conventional wind turbines AWESs offer some notable advantages. While conventional wind turbines require a tower structure to support the generator, gear box and rotor, an AWES replaces the components as well as the inner turbine blade sections by a tether. As the kite creates its own lift and a ground-based power station a support structure is not needed (Diehl *et al.*, 2013). This reduction in material also causes a decrease in construction work and time, resulting in a generally smaller

ecological footprint for a same sized generator (Khan and Rehan, 2016; Diehl *et al.*, 2013).

Additionally, for a conventional wind turbine more than half of the extracted wind energy is harnessed by the outer 30% of the turbine blades. These outer sections of the blades, also known as tips, are thin and light weight. This results in a mostly inefficient inner part of the turbine blades that makes up most of the blade's weight. The deployment of AWESs aims to tackle these inefficiencies by reducing most of the structure while only using the characteristics of the blade tips (Diehl *et al.*, 2013; Bechtle *et al.*, 2019). As depicted in Figure 1, the kite is simply defined as a flying wing, mimicking the blade tips of a turbine (Diehl *et al.*, 2013).

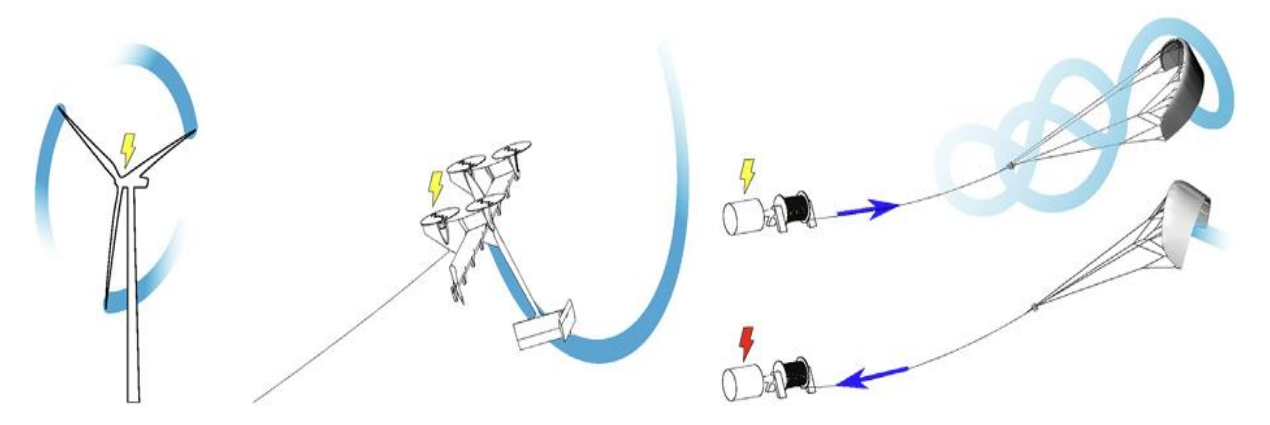


Figure 1: Comparison of rotor area of the tips of conventional wind turbines and the flight path of different AWES concepts with respect to power generation and structure

Source: [1]

It is important to note that this thesis will not discuss any economic aspects of AWESs. Since the focus lies on a research mission and the possibility of the use of AWES in the atmosphere of Mars as a potential power source thus, only a technological assessment will be made.

2.1.1 Classification

AWESs can be classified and categorised regarding several characteristics. The most general categorization revolves around the generation of electricity with further distinctions such as flight operation, kite structure, and control method to name a few possible (Cherubini *et al.*, 2015; Diehl *et al.*, 2013; Jochem Weber, Melinda Marquis, Aubryn Cooperman, Caroline Draxl, Rob Hammond, Jason Jonkman, Alexsandra Lemke, Anthony Lopez, Rafael Mudafort, Mike Optis, Owen Roberts, Matt Shields, 2021). So far, the AWE sector has not converged to a specific technology or concept resulting in numerous designs and different approaches being tested (Jochem Weber, Melinda Marquis, Aubryn Cooperman, Caroline Draxl, Rob Hammond, Jason Jonkman, Alexsandra Lemke, Anthony Lopez, Rafael Mudafort, Mike Optis, Owen Roberts, Matt Shields, 2021).

As for this thesis, three classifications important for this work are elaborated to characterise the AWES later used in the simulation. While this chapter does not aim to give a complete overview of all types of AWES, it should give an idea of the variety of designs of these kind of systems.

Electricity Generation

The positioning of the electricity generator is often used as the most general categorization for AWESs splitting all AWESs into two categories. The generation of electricity can take place on the ground (Figure 2a) or on board the kite (Figure 2b). The former is Ground Generation (GG), while the latter is referred to as Fly Generation (FG) with electricity generated on board the flying kite.

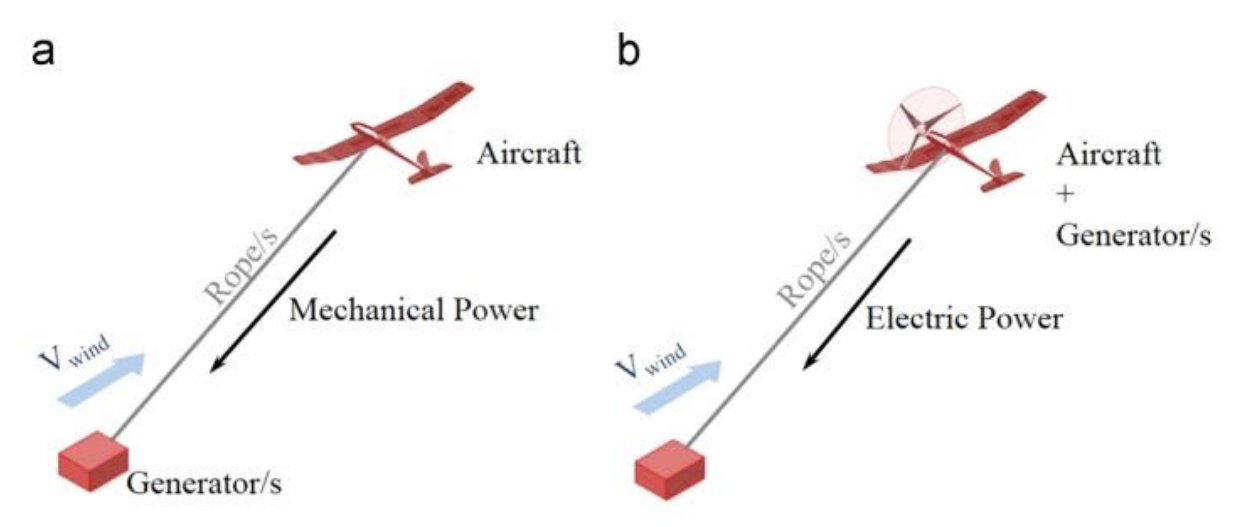


Figure 2: Distinction of AWESs concerning the position of the generator; (a) Ground-Generation; (b) Fly-Generation Source: (Cherubini et al., 2015)

Ground-Gen

AWESs using Ground Generation (GG) work by converting the lift force generated by the kite into a traction force using the attached tether. There are different concepts to realise this approach with the pumping cycle utilizing a drum-roll being the most used solution so far. Many companies in the Airborne Wind Energy industry are focussing on developing such a pumping cycle system as the simplicity and non-resource-intensive characteristic of the GG system are used to establish the commercialization of AWESs (Diehl *et al.*, 2013; Cherubini *et al.*, 2015; Jochem Weber, Melinda Marquis, Aubryn Cooperman, Caroline Draxl, Rob Hammond, Jason Jonkman, Alexsandra Lemke, Anthony Lopez, Rafael Mudafort, Mike Optis, Owen Roberts, Matt Shields, 2021).

Figure 3 shows an example of such a pumping cycle. In the ground station of the AWES, the tether force is converted into mechanical traction power by unravelling the tether from a drum roll connected to a generator (Figure 3a). By unravelling the tether

from the drum roll, the generator is set in motion to produce electrical energy. Since the tether length is limited, this kind of operation requires a cyclical approach as power can only be generated as the tether is unwind from the drum roll. Once the maximum tether length is deployed, the tether needs to be reeled-in again. This type of operation of reeling-out and reeling-in is called a pumping cycle. Since the reeling-in of the tether requires power itself, the kite is controlled and steered in a way to enable an efficient retraction of the tether requiring less energy than is produced to generate a net-plus of energy during the cycle (Figure 3b). As the pumping cycle does not generate continuous power the ground station needs to incorporate an energy storage such as a battery or capacitor to be used as a non-fluctuating source of electricity (Jochem Weber, Melinda Marquis, Aubryn Cooperman, Caroline Draxl, Rob Hammond, Jason Jonkman, Alexsandra Lemke, Anthony Lopez, Rafael Mudafort, Mike Optis, Owen Roberts, Matt Shields, 2021; Diehl *et al.*, 2013).

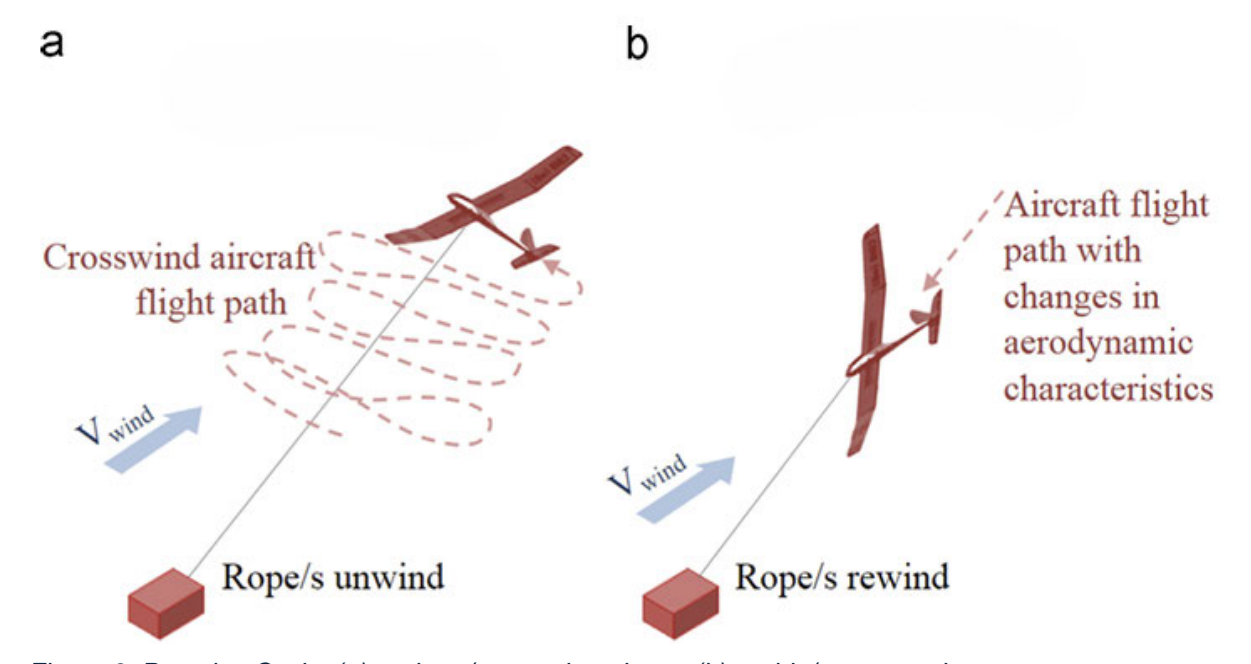


Figure 3: Pumping Cycle; (a) reel-out/generation phase; (b) reel-in/recovery phase Source: (Cherubini et al., 2015)

Ground Generation does not necessarily equal a stationary ground station. Instead of reeling-in and -out the tether, a component or the ground station itself is set in motion to generate electricity. However, no prototype has been developed so far, with the main disadvantages being the increased complexity as well as the necessary resources (Cherubini *et al.*, 2015; Bechtle *et al.*, 2019; Jochem Weber, Melinda Marquis, Aubryn Cooperman, Caroline Draxl, Rob Hammond, Jason Jonkman, Alexsandra Lemke, Anthony Lopez, Rafael Mudafort, Mike Optis, Owen Roberts, Matt Shields, 2021).

Fly-Gen

Fly-Gen, On-board Generation, or FG mostly integrates energy generating devise such as turbines mounted to the kite itself. The tether stays at a constant length during the operation with no cyclical retraction allowing the on-board generators to produce electricity continuously in flight and during operation (Khan and Rehan, 2016; Cherubini *et al.*, 2015; Diehl *et al.*, 2013). Since the on-board turbine or power generator results in extra drag for the aerodynamics of the kite, Miles Loyd called it drag mode (Loyd, 1980).

The tether acts as a cable conducting the on-board generated electricity to the ground station and further to the grid. The continuous generation of electric power does not require an energy storage facility such as the GG approach, while also eliminating a necessary gearbox as the turbines are able to operate with high rotational speeds increasing their efficiency. An additional advantage of the application of turbines are their possible dual use for landing and take-off (Diehl *et al.*, 2013; Khan and Rehan, 2016). Different concepts of systems by companies utilising the FG approach are depicted in Figure 4.

However, the FG concept inherits some downsides. To achieve high energy yields, the kite needs to achieve high speeds for the optimal operation of the mounted turbines. High kite speeds lead to high tensions in the tether through increased lift, and a high drag coefficient of the tether. To minimise power losses and enable an efficient power transfer, the cable needs to be well insulated, increasing the tether diameter thus further increasing its drag. For a flying wing with high efficiency airfoils

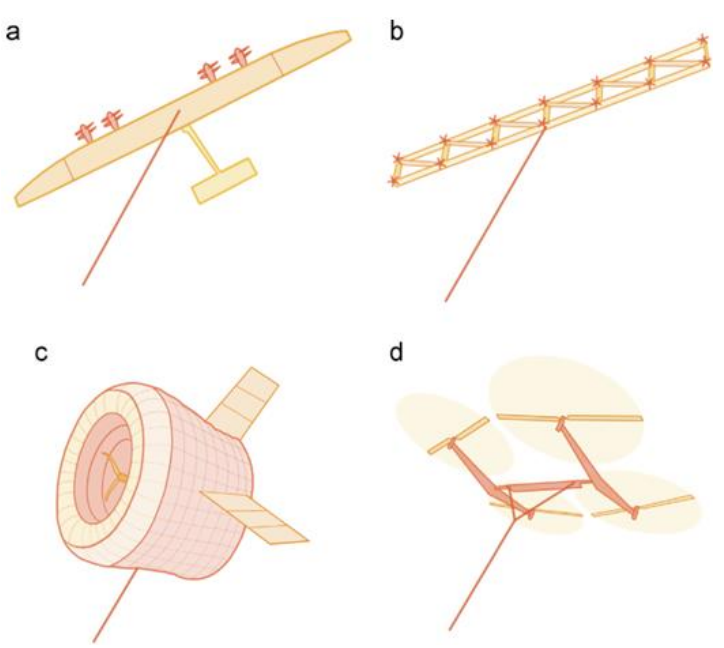


Figure 4: Kite concepts utilising on-board electricity generation;(a) plane with turbines;(b) airframe with wings and turbines; (c) Aerostatic balloon with centre turbine; (d) autorotational quadcopter Source: (Cherubini et al., 2015)

the tether can be the biggest contributor to the system's overall drag. Additionally, the on-board mounted power generators increase the overall weight of the kite, making it more difficult for take-off and staying airborne (Diehl *et al.*, 2013).

A sub-division of the FG category is the "Lighter-than-Air"-approach. In this concept the necessary lift for the kite to stay afloat is generated using aero-static lift via a volume of gas, that is lighter than air. These types of systems are very dependable on the atmospheric conditions to enable operation. The temperature and pressure of the surrounding air impacts the achievable height and thus the effectivity on the system. Gas leakage over time leads to increased downtime (Diehl *et al.*, 2013). In the 2021 report from the National Renewable Energy Laboratory, this approach is noted as being "less promising and [...] no longer widely pursued." (Jochem Weber, Melinda Marquis, Aubryn Cooperman, Caroline Draxl, Rob Hammond, Jason Jonkman, Alexsandra Lemke, Anthony Lopez, Rafael Mudafort, Mike Optis, Owen Roberts, Matt Shields, 2021)

Flight Operations

Crosswind

Although Loyd was the first to theorise about the use of kites to generate power, as described above, he only mentioned the method using a crosswind motion of the kite. The first publication on the use of AWES for energy extraction specifically describes the use of a kite flown perpendicularly to the direction of the wind (Loyd, 1980). This enables the kite to achieve significant velocities, much higher than the prevailing wind speed being beneficial for GG and FG systems alike. On one hand the quadratic relation between speed and lift force results in a high tether tension during the reel-out phase, on the other hand, high wind speeds lead to high electricity output of onboard mounted turbines. A significant downside to the crosswind operation is the aerodynamic tether drag that increases with the velocity of the kite.

Operating in crosswind motion enables the scalability of AWESs and power generation of up to two orders of magnitude higher than systems operating in non-crosswind motion (Cherubini *et al.*, 2015). This has led to crosswind operations being the most pursued approach for companies. Almost all crosswind trajectories follow a circular or figure-of-eight flightpath, with the figure-of-eight being the most prevalent (Cherubini *et al.*, 2015). Systems following a circular trajectory need to address the resulting twisting of the tether (Diehl *et al.*, 2013).

Non-Crosswind

As already mentioned, systems using non-crosswind operations exhibit a significant lower power output. While not going in depth, there are approaches such as the lighter-than-air designs as well as the autorotating multi-copter concepts being tested and deployed. Further concepts utilise drag forces, such as the ladder mill, with several

soft kites acting like parachutes to generate traction force (Ockels, 2001). Another approach is based on the Magnus effect (Perković *et al.*, 2013). The focus of this thesis, however, will be crosswind operations since they are the most deployed and used systems also offering a higher potential for commercial applications. The next category presented in this chapter concerns the differentiation of the kite's structure, ranging from rigid airframes to parafoils similar to surf kites.

Kite Structure

Below the aforementioned two classification levels, further differences between concepts can be identified based on the kites' properties, the launch-and-landing approaches as well the number of kites to name a few. Concerning the structure of the kite, the categories include rigid and flexible wings with multiple sub-categories and hybrid designs. Hybrid systems incorporating rigid and flexible elements to combine advantages are also being developed but will not be further discussed in the thesis. Some of the different rigid and soft kite designs are shown in Figure 5. In the following, the main advantages and disadvantages of completely rigid airframes and soft, flexible kites are presented.

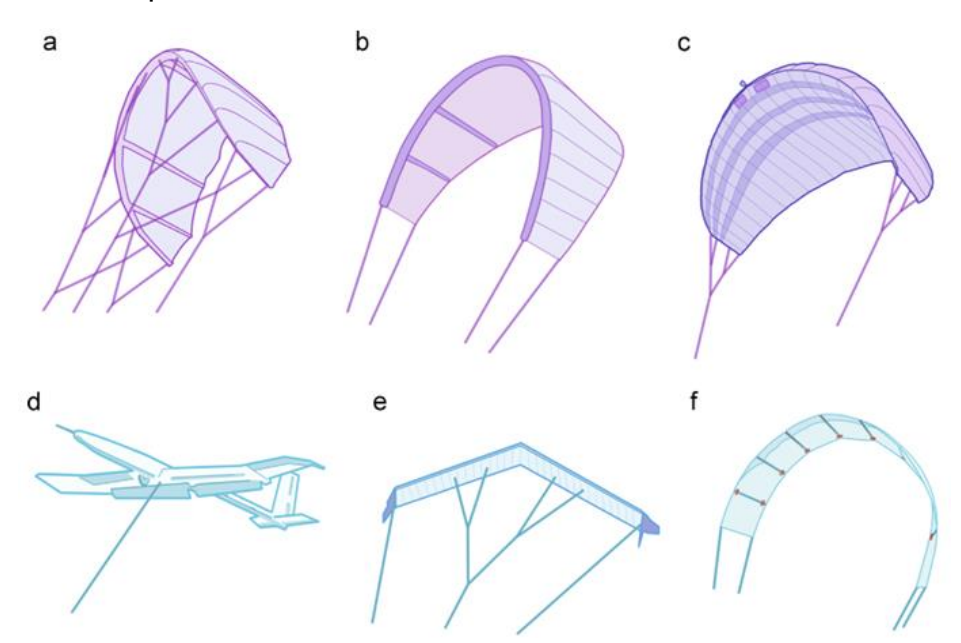


Figure 5: Several rigid and soft kite designs for Ground Generation; (a-c) soft and flexible kite designs; (d, e) rigid wing designs; (f) semi-rigid wing

Source: (Cherubini et al., 2015)

Rigid Wing

Rigid wing kites act like flying wings with the airfoils geometry not being dependable on the ambient air conditions. This design generally exhibits a higher lift-to-drag-ratio compared to soft kites enabling an operation with higher velocities leading to a higher energy output per wing area. As higher velocities result in higher lift forces, a GG-system can achieve higher power yields. When used in an FG system, the higher velocities also benefit the use of power generators such as turbines (Diehl *et al.*, 2013; Loyd, 1980).

Different methods for control implementation are depicted in Figure 6. Rigid wings are either controlled using actuators for ailerons, elevators, and rudders Figure 6. Further, kites can also be steered using bridles, or even lines connected to the ground station (Figure 6a). Bridle lines are used for steering by changing their length accordingly using a control pod positioned between tether and bridles (Figure 6b). However, the kite can also be steered from the ground using the tether and or control lines (Figure 6c and d) Some publications use the number of bridle lines as another means to categorise AWESs (Cherubini *et al.*, 2015; Jochem Weber, Melinda Marquis, Aubryn Cooperman, Caroline Draxl, Rob Hammond, Jason Jonkman, Alexsandra Lemke, Anthony Lopez, Rafael Mudafort, Mike Optis, Owen Roberts, Matt Shields, 2021).

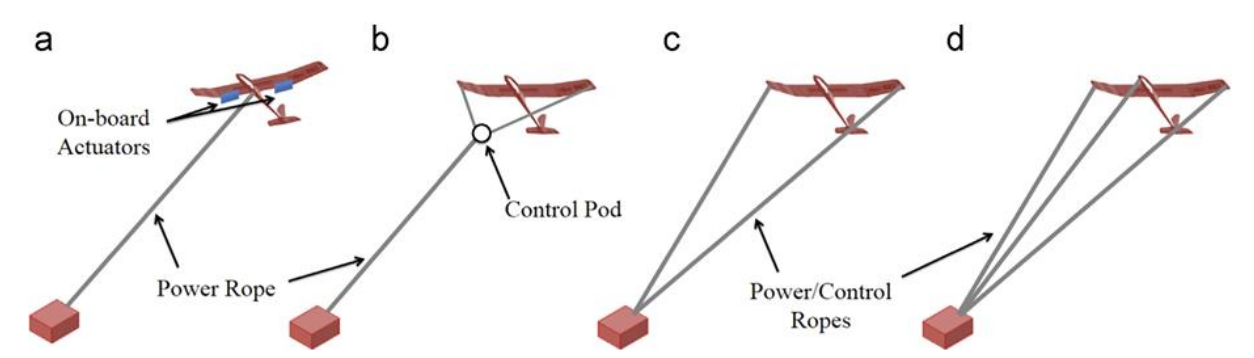


Figure 6: methods for kite control; a) deflectors on-board; b) control unit for bridle lines; c and d) usage of power and control lines Source: (Cherubini et al., 2015)

Flexible Wing

While rigid wing design promise a larger scalability of AWESs, the first applications of AWESs deploy a flexible wing design, which inherit lower safety risks and easier handling. Bridle lines enable the control of soft kites. Depending on the alignment and number of bridle lines various flight parameters can be varied (Cherubini *et al.*, 2015).

Kites utilising a flexible membrane as a lift generator have been in use for decades and are used in various fields. Flexible wing designs or soft kite approaches can be divided by the kite structure, the level of structural elements and the number of bridle lines. Unlike rigid wing design, the kite's shape depends on the atmospheric parameters and the resulting aerodynamic load distribution. They are lightweight for a given surface area leading to a high specific power density (Diehl *et al.*, 2013).

Overall, the widespread utilisation of AWESs has several challenges yet to overcome. Areas with remaining questions involve safety, reliability, durability, and environmental impact. During operation the kite must stay airborne, which can lead to safety issues as an immediate halt of operations in case of an emergency is not easily possible. Furthermore, since a high kite velocity is beneficial for power extraction, crashes as well as the fast-moving tether pose a potential danger to the imminent surrounding (Cherubini et al., 2015; Salma et al., 2020). Additionally, the components, in case of GG especially the tether, need to withstand many cycles of reeling-in and reeling-out with varying loads requiring high levels of durability. The fully autonomous operation of an AWES is still a major challenge (Cherubini et al., 2015; Salma et al., 2020). While the in-flight control mechanics are steadily approaching this goal, the automation of take-off and landing poses difficulties with reliant mechanisms not yet established (Watson et al., 2019). While studies have concluded that an extensive extraction of wind energy can alter the global climate and its dynamics, the limit for this is an order of magnitude of terra watts higher than the total, currently harvested wind energy today (Bechtle et al., 2019).

2.1.2 Wind Energy and Power

In this chapter, all equations needed to calculate the expected power output of an AWES are introduced as well as the fundamental aerodynamic influences on the dynamics of the kite. The following equations presented in this chapter are mostly based on (Diehl *et al.*, 2013) and (Schmehl *et al.*, 2024).

In order to understand the AWESs and their operation, a general mathematical description of their means of power generation is needed. Calculating the power output by a given AWES requires an analytic understanding of wind power overall. The equation for calculating the wind power is derived from the kinetic energy of the mass flow of air through a given cross section A. For conventional wind turbines A equals the rotor swept area, while for AWESs it corresponds to the total area the kite covers during its flight path. Expressing the mass flow as a volume resulting from air flowing through A at the speed of v_w multiplied by its density leads to equation (1).

$$P_W = \frac{1}{2} * \rho * A * v_w^3 \tag{1}$$

By dividing the expression for wind power by the area, the wind power density (WPD) is obtained (2). By defining the maximum power production per unit area, the WPD enables a comparison of different systems in the given wind conditions (Hartwick *et al.*, 2023).

$$\frac{P_W}{A} = \frac{1}{2} * \rho * v_w^3 \tag{2}$$

During flight, the kite generates a lift and drag force. By adding both force components, the resulting aerodynamic force depends on the wing area S, the apparent wind speed of the kite v_a , and the resultant total aerodynamic force coefficient of the kite C_R as well as the air density ρ (3). The apparent wind speed is the speed of the incoming air flow relative to the kite.

$$F_a = \frac{1}{2} * \rho * v_a^2 * C_R * S \tag{3}$$

The coefficient C_R derives from the relation between the kite's lift, its drag forces, and the resulting aerodynamic force of the kite in (4), with the corresponding lift and drag coefficients C_L and C_D . The drag coefficient includes the drag of the kite itself as well as the tether drag in addition to potential sources of drag such as mounted turbines for FG operations.

$$C_R = \sqrt{C_L^2 + C_D^2} \tag{4}$$

To calculate the maximum usable power an AWES can generate the optimal ratio of the kites' apparent speed to the wind speed is determined. This leads to the equation for the maximum usable power produced by an AWES for a given wind speed v_w in (5).

$$P_{max} = \frac{2}{27} * \rho * A * v_w^3 * C_R * (\frac{C_L}{C_D})^2$$
 (5)

The equations and conclusions mentioned above are valid for all types of AWES. For the rest of this chapter, the power generation and the calculated power output of a ground generating system operating in a pumping cycle will be discussed. The choice of the system type will be discussed in the following chapter concerning the methodology. For now, several assumptions and consideration to simplify the calculations are introduced.

Power Generation of a Pumping Cycle

As later explained, due to the light weight of the simulated kite and the lower gravitational acceleration of Mars, gravitational effects and influences of inertia are neglected. Furthermore, the equations will not consider the azimuth angle between wind speed direction and the tether orientation in the horizontal plane. This results from the assumption that except from small deviations during manoeuvring the kite operates in the same plane at an azimuth angle of 0° relative to the direction of the

wind speed (Schmehl *et al.*, 2024; Diehl *et al.*, 2013). Figure 7 depicts the trajectory of a kite during a pumping cycle. The pumping cycle is broadly separated into two phases, the traction phase marked with the index "out" and the retraction phase marked with the index "in". To calculate the power output of a cycle the transition phases are neglected as an optimised flight path aims to minimise these phases (Schmehl *et al.*, 2024). The following equations are based on several assumptions. Since the elevation angle β between a theoretical straight tether under tension and the ground plane oscillates around an average value, the elevation angle during reel-out is approximated to be a constant β_0 . This leads to a constant β during reel-out as well as a constant elevation angle β_1 during reeling-in, characterizing both phases. The same is considered for the lift coefficients, with a maximised $C_{L,out}$ and a minimised $C_{L,out}$. Further, the phases are constrained to the maximum and minimum deployed length of the tether, r_{max} and r_{in} respectively. Since the wind speed varies with altitude, the wind speed at the average altitude $z_{m,0}$ is used .

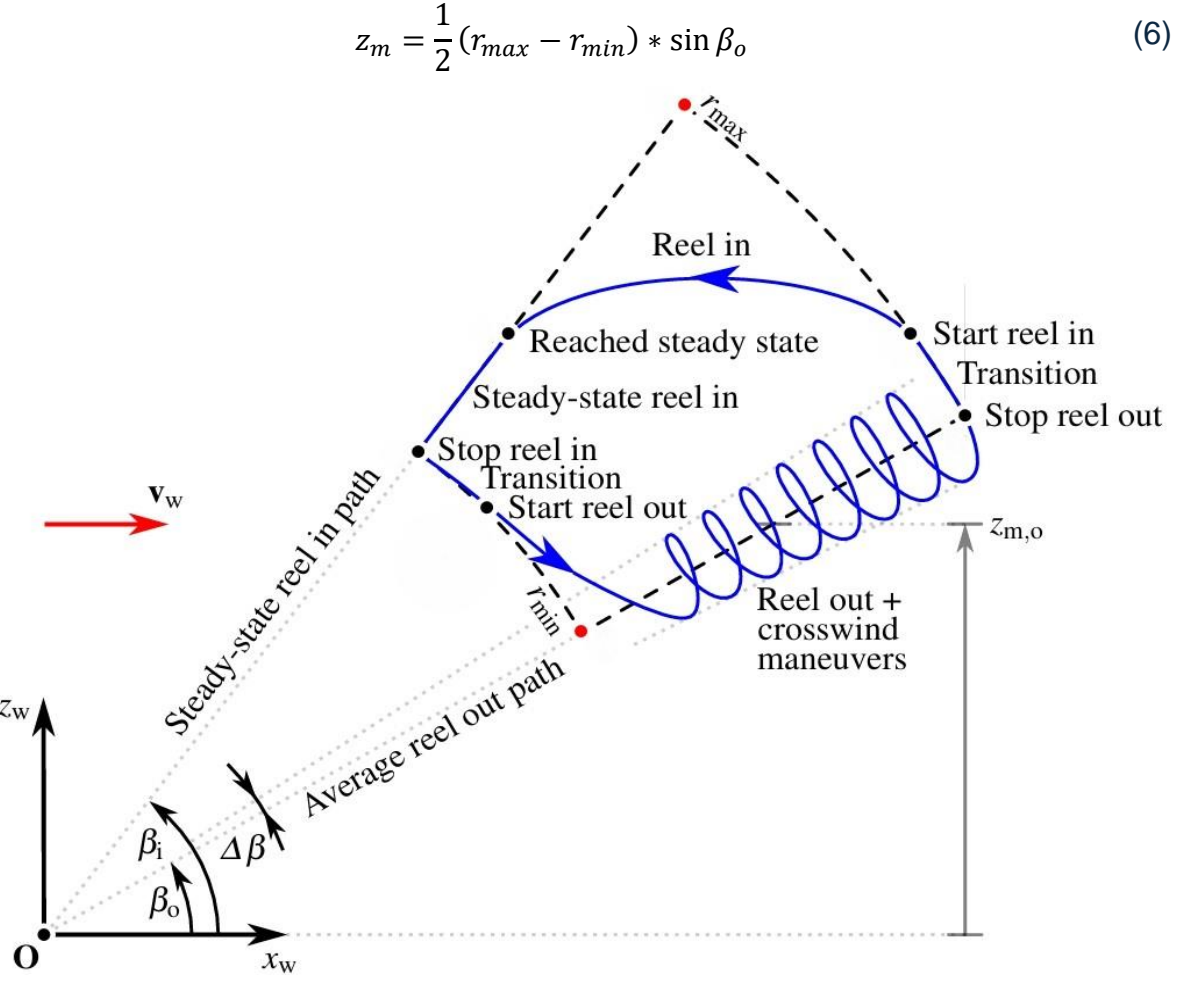


Figure 7: Real (blue line) and idealised (dashed line) flight path during a pumping cycle with the elevation angles during reeling Source: (Schmehl et al., 2024)

Reel-Out

The mechanical or traction power P_{mech} is calculated by multiplying the traction force T equal to the aerodynamic force F_a acting on the kite with the traction speed $v_{t,out}$ (7).

$$P_{mech} = T * v_{t,out} = F_a * v_{t,out} \tag{7}$$

Loyd concluded in his first paper concerning AWESs that an optimal tether velocity of one third of the wind speed maximises the mechanical power (Diehl *et al.*, 2013; Loyd, 1980).

Since the tether length is not constant, the kite's speed also depends on the velocity with which the kite is reeled-in and -out. This is accounted for by defining the reeling factors f_{in} and f_{out} according to the phase as the normalised tether velocity v_t (8).

$$f_{in/out} = \frac{v_{t,in/out}}{v_w} \tag{8}$$

With the additional motion in tether direction, the kite's apparent speed is altered and dependent on the cycle phase. This leads to the apparent speed to be expressed as in equation (9) with respect to the wind speed, the lift-to-drag ratio E, the elevation angle β , and the reeling factor f.

$$v_a = v_w * \sqrt{1 + E_{out}^2} * (\cos \beta - f)$$
 (9)

By expressing the resultant aerodynamic coefficient with the lift-to-drag ratio as well as the lift coefficient during the reel-out phase the traction force and the resulting traction power generated are calculated using equation (10).

$$T_{out} = \frac{\rho}{2} * v_w^2 * A * C_{L,out} * \sqrt{1 + \frac{1}{E_{out}^2}} * (1 + E_{out}^2) * (\cos \beta_o - f)^2$$
 (10)

While the lift-to-drag ratio depends on the design choices, both beta_in and the reeling factor f_in are controlled by the ground station.

Reel-In

To attain the power output over a complete cycle of traction and retraction of the tether the reel-in phase and the necessary power are calculated. To ensure an easy control and steady descent during the reel-in phase, the elevation angle is kept constant. For the apparent speed with no tangential component as the kite is drawn towards the ground station this leads to equation (11).

$$v_{a,in} = v_w * \sqrt{1 - 2 * f_{in} * \cos \beta_i + f_{in}^2}$$
 (11)

The tether force during the reel-in phase is determined by equation (12).

$$T_{in} = \frac{\rho}{2} * v_w^2 * A * C_{L,in} * \sqrt{1 + \frac{1}{E_{in}^2}} * (1 - 2 * f_{in} * \cos \beta_{in} + f_{in}^2)$$
 (12)

Now that the equations of the corresponding traction forces during the phases have been established, the net output of a complete cycle can be defined. First, the amount of work is determined by multiplying the acting forces along the distance travelled by the kite which is set as the difference between the maximum tether length after reeling-out and the minimum length after the reel-in phase (13).

$$E_{cycle} = [T_{out} - T_{in}] (r_{max} - r_{min})$$
 (13)

The net power output results by dividing the energy by the cycle duration, expressed using the maximum and minimum tether length, as well as the reeling factors, and the wind speed (15). In this equation, both reeling factors are treated as positive numbers.

$$t_{cycle} = \frac{(r_{max} - r_{min})}{v_w} * \frac{f_i + f_o}{f_i f_o}$$
 (14)

The only atmospheric parameters necessary to calculate the power output of an AWES operating in a pumping cycle are the wind speed and atmospheric density. However, to describe the dynamics of a planetary atmosphere, a general understanding of the large- and small-scale factors influencing the atmospheric conditions is necessary. The following chapter aims to introduce the Red Planets atmosphere as well as its phenomena specific to Mars.

2.2 Mars

Mars is Earth's outer neighbour and has been observed by scientists for centuries. Since the early 1960s modern Mars exploration has begun and resulted in the first spacecrafts, Viking I and II landing on the so-called red planet in 1976 (Sánchez-Lavega *et al.*, 2024). Since then, several satellites have been and still are orbiting Mars as well as several missions deployed to explore the planet from the surface. Mars has a radius of around 3390 km, making it almost half the size of Earth. The Martian orbit exhibits a noticeable eccentricity of 0.0935, leading to a change of distant from 207 million km at perihelion to about 250 million km at aphelion from the sun (SMD Content Editors, 2024; Sánchez-Lavega *et al.*, 2024). With a tilt angle of 25.2°, it is greater than Earth's 23,4° (Martínez *et al.*, 2017). A Martian year, a full orbit around the sun, takes 687 Earth days or 668.6 Martian days. These days, also referred to as sols, are approximately 24h and 39min long (Martínez *et al.*, 2017). The planet appears reddish in colour due to the oxidized iron in the rocks and soil covering the surface. In Figure 8 a colourised topography of the red planet is depicted. It also includes markings of the landing sites of several Mars missions to give some kind of orientation.

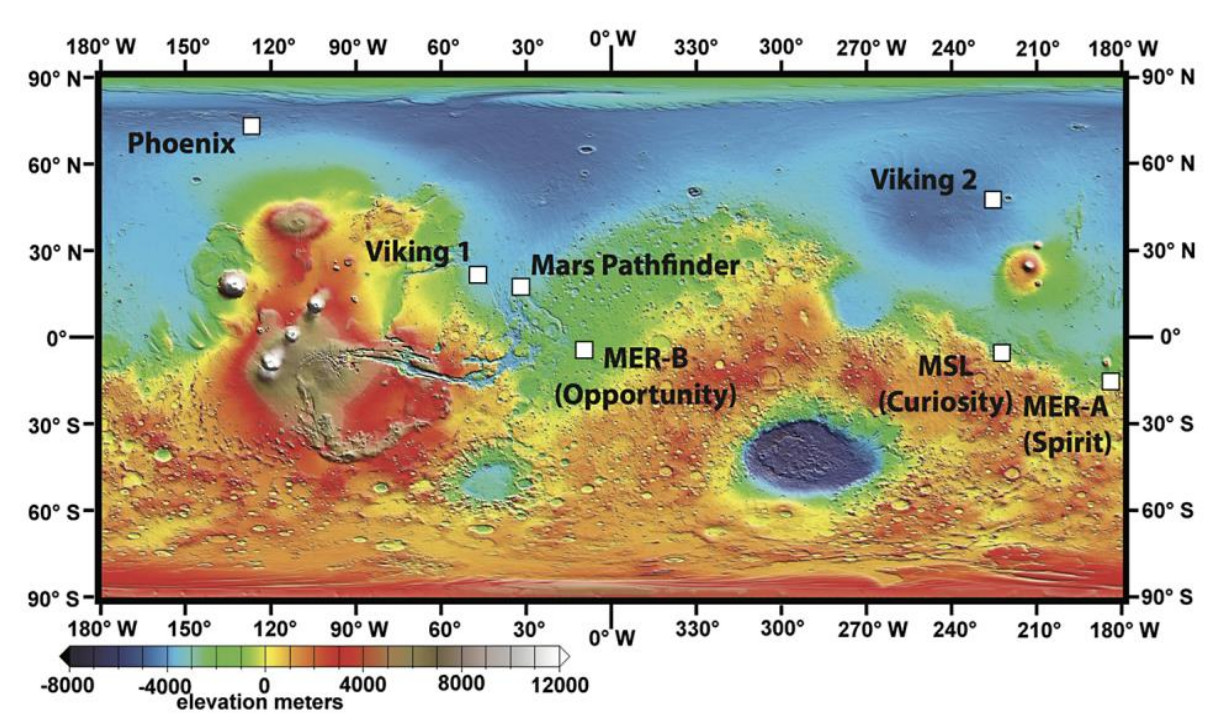


Figure 8: colourised topography of the Martian surface including landing sites of Martian lander missions

Source: [15]

The rocky terrain is characterised by volcanos, mountains, plateaus, canyons, and basins (Zhao *et al.*, 2023). With evidence of a former presence of liquid water such as stream beds and significant quantities of hydrated minerals, the lack there of today results from atmospheric escape of hydrogen and oxygen. This steady depletion of

"the building blocks of water" is assumed to be one of the primary factors of Mars' climatic evolution over the solar system's history— from an atmosphere enabling the presence of liquid water to a scarce and dry atmosphere (Almatroushi *et al.*, 2021).

The following chapters will introduce and discuss the atmospheric dynamics of the lower atmosphere such as the composition and its different climatic cycles. This allows a later assessment of potential wind energy harnessing in the lower atmosphere utilising an AWES. Furthermore, a short history on the development of sufficient Martian climate models is included as well as the current models used to attain the needed data for this thesis.

2.2.1 The Martian Atmosphere

The thin Martian atmosphere is comprised of mainly carbon dioxide, at 95%, with traces of nitrogen, argon, oxygen, and carbon monoxide with an atmospheric density of about 1/70 of Earth's atmosphere (Zhao *et al.*, 2023; Almatroushi *et al.*, 2021).

There are two main temporal cycles that significantly influence the atmospheric parameters and dynamics. The annual or seasonal cycle derives from the orbital eccentricity and the Martian orbital tilt while the diurnal cycle describes the variation between day and night on Mars (Sánchez-Lavega et al., 2024; Almatroushi et al., 2021). Just like its earthly neighbour, the Martian climate is characterised by seasons resulting from its position relative to the sun. This seasonal cycle is caused by the change of the distance between Mars and the sun and its tilt angle in respect to the orbital plane. Unlike on Earth, the seasons significantly differ in terms of duration due to the orbit's eccentricity. In Figure 9 the trajectory of Mars around the sun is shown divided into 12 Martian months of 30° each. For reference, the northern hemisphere summer solstice occurs at 90° solar longitude and winter solstice at 270° solar longitude. The diurnal cycle refers to the day-night shift. Since the atmosphere is so thin it enables high levels of radiation to reach the Martian surface causing significant surface temperature differences between day and night as well as significantly influencing the thermal structure of the lower atmosphere (Almatroushi et al., 2021). The lower atmospheres dynamics depend mainly on the behaviour of CO₂, water vapor and dust resulting from seasonal and diurnal fluctuations (Peng et al., 2023). Further factors are radiative and dynamical processes closely linked to these cycles (Martínez et al., 2017). Due to the predominant temperature and pressure regimes, the CO₂ in the atmosphere sublimates at the poles during their respective winter season causing roughly 30% of the atmosphere's CO₂ being cycled annually through these seasonal polar caps. These periodic formations of CO₂ depositions are caused by the eccentricity of the orbit as well as its tilt (Martínez et al., 2017).

The second influential cycle is the dust cycle. Dust is always present in the Martian atmosphere with its quantity being spatially and temporally dependent, impacting the

local surface temperatures. On one hand, it increases opacity, reducing the sun's radiation reaching the surface, on the other hand it radiates heat itself, changing the heating rates of the atmosphere and surface.

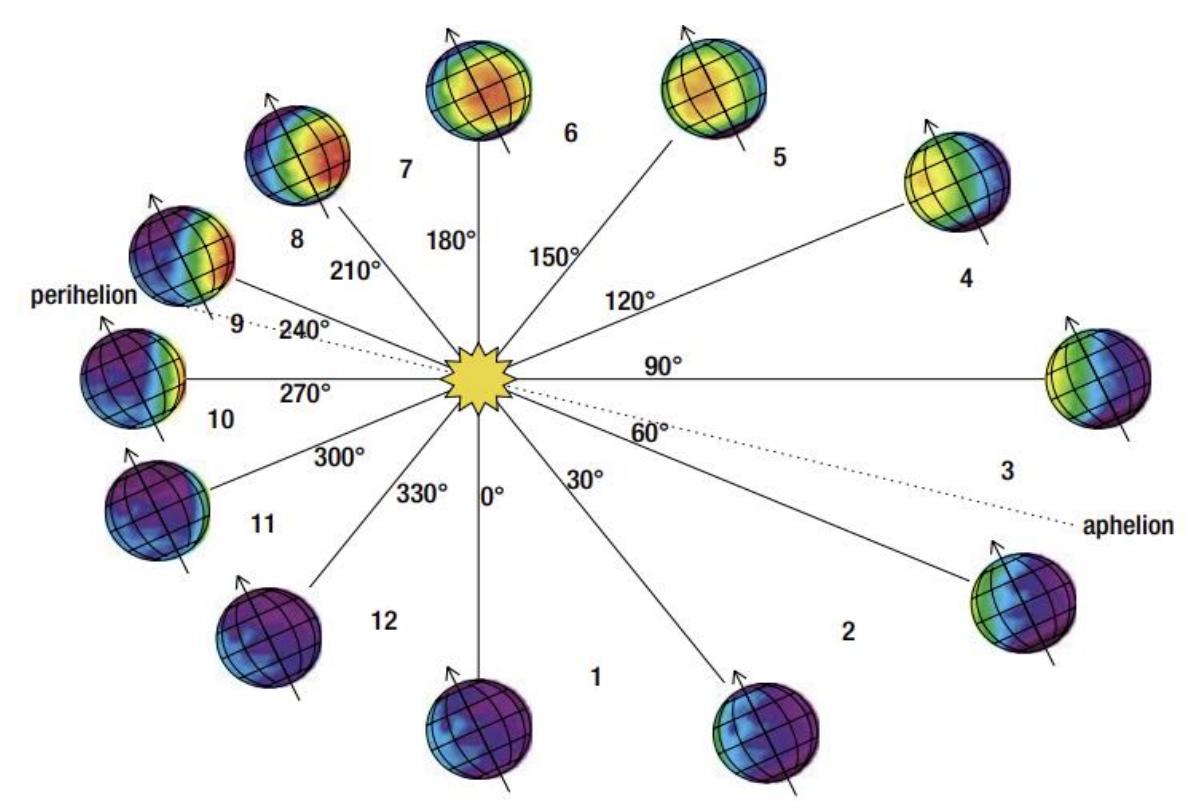


Figure 9: solar longitudes of the martian orbit with exaggerated eccentricity; colorization according to day-time surface temperature ranging from 40K (deep purple) to 315K (bright red)
Source: (SMD Content Editors, 2024)

The H₂O cycle also undergoes seasonal changes leading to formation of ice depositions and ice clouds in the atmosphere (Martínez *et al.*, 2017). Water is presumed to be present beneath the surface in the form of ice. All the factors mentioned above alter the global and local atmospheric conditions. These circumstances plus local topography influence the wind speed.

Phenomena of the Martian Climate

Climatic phenomena on Mars occur from a small scale like dust devils similar to Earth's up to global scale dust storms. These global dust storms can cover the planet's surface with dust for two to three months. Since dust plays such an important role in the climate the Martian year can be divided into the non-dusty season, from ca. 0° to 180° and the dusty or dust storm season beginning at around 180° and lasting to 360° of solar longitude (ESA *et al.*, 2006). Dust Storms on Mars are categorised in local, regional, and global dust storms. During the so-called dusty season both hemispheres experience dust storms at similar rates. The dusty season is during the southern spring/summer season (Almatroushi *et al.*, 2021; Sánchez-Lavega *et al.*, 2024). The

southern hemisphere is where most of the dust storms form (Almatroushi *et al.*, 2021). During perihelion season (southern spring and summer) the Martian climate can be affected by Global Dust Storms (GDS) or Planet Encircling Dust Storms (PEDS). In the last 62 years only eight GDS have been observed, covering the surface of the Red Planet in dust for 2-3 months (Sánchez-Lavega et al., 2024). The scale of such a GDS is shown in Figure 10 depicting the GDS in 2018 enveloping the planet and resulting in the loss of contact with NASA's Opportunity rover. Other atmospheric phenomena on a smaller scale also occur such as dust devils and cyclones affecting the local and regional dust distribution (Martínez *et al.*, 2017).

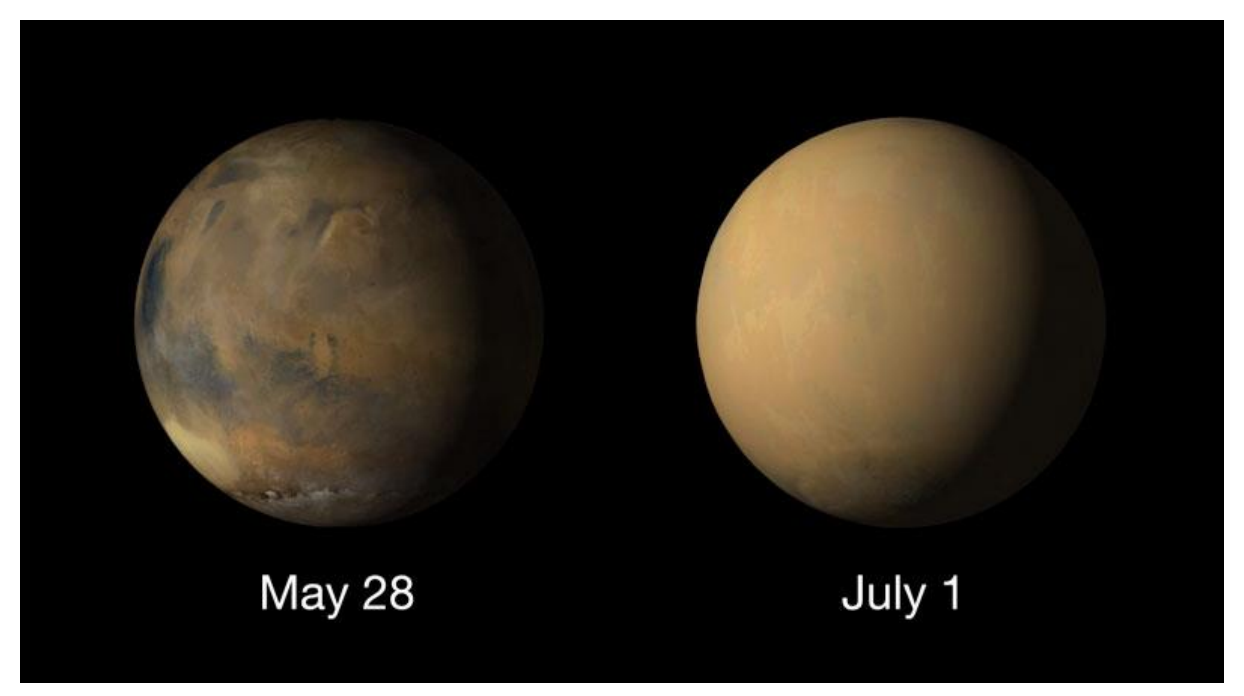


Figure 10: Example of the impact of a GDS in 2018

Source: NASA/JPL-Caltech/MSSS

2.2.2 Wind Energy on Mars

The main source of power on space missions is solar based. With the thin Martian atmosphere interfering little with the incoming solar radiation, solar panels are considered for energy support of manned- and unmanned missions alike. However, as discussed in the previous chapter, atmospheric phenomena and cyclic events, specifically concerning the dust cycle, can severely limit the solar power yield. For a manned mission requiring about 576-840 kWh per sol to support a crew of six this poses a serious threat. Therefore, research on back-up systems has emerged, with the implementation of wind power being one of them (Schorbach and Weiland, 2022; Hartwick *et al.*, 2023).

As already described in chapter 2.1, the achievable power yield of wind is proportional to its density and its velocity cubed. On one hand, the Martian atmosphere has a low density decreasing the potential power output of any wind energy generation system. On the other hand, large areas of the Martian surface are exposed to higher wind speeds than Earth, making wind energy a sustained and stable energy resource (Hartwick et al., 2023; Gaunaa et al., 2024). As of now, most of the scientific papers on wind energy on Mars revolve around a hybrid system, incorporating potential wind energy harnessing as a back-up for solar during low atmospheric opacity as apparent during the dusty season and as a back-up during nighttime (Ouroumova et al., 2021). It is also discussed utilising wind power for missions close to the poles to compensate for the lower solar radiation intensity, thus increasing the explorable areas (Hartwick et al., 2023). In general, there is a consensus about the possibility of generating power using wind energy systems in general (Hartwick et al., 2023; Schmehl et al., 2024; Schorbach and Weiland, 2022). Research analysing the measurements of the lander sensors as well as data collected from global climate models have been published further acknowledging the potential of wind energy (Hartwick et al., 2023; Schorbach and Weiland, 2022; Ouroumova et al., 2021). However, data not based on measurements is limited in scale and accuracy as later explained. Furthermore, shortterm variations and influences of the local topography cannot be captured (Hartwick et al., 2023).

Through all the calculated values and assumptions based on output of an atmospheric model that is later discussed in depth, several non-calculable factors need to be considered. Since wind power is proportional to the to the wind speed cubed, the error margin for the estimated and or expected wind power can grow quite large. Further, wind speeds are not constant but volatile and influenced by a multitude of factors, fluctuating on a scale of seconds and meters. At last, the environment of the Red Planet such as extreme temperatures and high dust contents in the air can lead to high rates of electronic and mechanical failures from resulting abrasion and mechanical or thermal fatigue (Zhao *et al.*, 2023).

With these considerations concerning all wind energy systems including wind turbines and AWES, an approach is introduced specifically for soft kite systems to account for the physical differences between Earth and the Red Planet. To enable an analysis of the different atmospheric influences on kite systems, Schmehl et al. have published a paper "...[i]nvestigating how far the physics of tethered flight differs on the two planets, specifically from the perspective of airborne wind energy harvesting" (Gaunaa *et al.*, 2024).

In the publication, the differences of the physical properties of the atmospheres are accounted for by implementing scaling factors (Gaunaa *et al.*, 2024). These are based on two requirements and two basic assumptions to adapt a soft kite system operating

on Earth to also be deployed on Mars. Under the conditions of an equal power output and the same building materials as well as their properties, the scaling factors include the kite's geometry, the tether characteristics, manoeuvrability, and the physical parameters.

The two basic assumptions are the following:

 The aerodynamic lift and drag coefficient are the same for the kite on Earth and Mars:

$$C_{L.Mars} = C_{L.Earth}$$

and

$$C_{D,Mars} = C_{D,Earth}$$

2. The average elevation angle is identical for the operation on Earth and Mars:

$$\beta_{Mars} = \beta_{Earth}$$

The first assumption is based on the dimensional analysis of the aerodynamic coefficients. It leads to the conclusion, that C_L and C_D are only dependent on the non-dimensional quantities of the airfoil shape, such as the angle of attack in the cross-sectional plane, the apparent Mach number and Reynolds Number. The second assumption concerning the same average elevation angle derives from as equal power coefficient of the original earth system and the scaled Mars system.

As stated in (Gaunaa *et al.*, 2024) the introduced scaling factors are based on the density and wind speed ratios of the two planets, as presented in (15) and (16).

$$K_{\rho} = \frac{\rho_{mars}}{\rho_{earth}} \tag{15}$$

$$K_{vw} = \frac{v_{w,mars}}{v_{w,earth}} \tag{16}$$

For the altered geometry of the kite, the planform area of the kite needs to be significantly larger than on Earth in order to match the power coefficient. Based on the assumption of a similar aspect ratio the scaling factors for the planform area S and the wingspan b are given in (17) and (18).

$$K_S = \frac{S_{mars}}{S_{earth}} = \frac{1}{K_\rho * K_{\nu w}^3}$$
 (17)

$$K_b = \frac{b_{mars}}{b_{earth}} = \frac{1}{\sqrt{K_\rho * K_{vw}^3}}$$
 (18)

Based on an equal power coefficient and the use of the same materials an equal tether stress is concluded. Further assuming a lower tether force, the resulting scaling factor of the tether diameter is derived in (19). This leads to a decrease of the tether drag coefficient, as stated in (Gaunaa *et al.*, 2024).

$$K_d = \frac{1}{\sqrt{K_{vw}}} \tag{19}$$

The mass of the kite is proportional to the volume and the density of the material. The volume of the kite equals the planform area S times the membrane thickness t. With a resulting reduction of the membrane thickness, the kite mass ratio of Mars to Earth is given in (20).

$$K_m = \frac{1}{\sqrt{K_\rho * K_{vw}^5}}$$
 (20)

With a scaling of the dimensions, the nominal tether force is altered too. Even though Mars exhibits higher wind speeds, the expected tether force decreases by the scaling factor K_F (20). The lower exerted force is compensated by a larger reel-out speed, according to (Gaunaa *et al.*, 2024).

$$K_F = \frac{1}{K_{max}} \tag{21}$$

The change in manoeuvrability is determined to be proportional to the change in the turning radius R of the kite (Gaunaa *et al.*, 2024). Based on the kites' ability to turn using the same steering input, the ratio of the turning radius with respect to the wind speed and density factors is given in (22).

$$K_R = K_{\nu\nu}^2 \tag{22}$$

As for parameters involving atmospheric conditions such as the Mach and Reynolds Number as well as specific aerodynamical properties of the kite, these are not investigated in this thesis as it is beyond the scope of this work requiring extensive wind tunnel testing and appropriate kite design choices.

With the scaling factors depending on the prevailing densities and wind speeds this ultimately leads to the question of a suitable site of deployment for a scaled AWES. If the AWES is supposed to support a manned-mission further factors need to be considered. NASA as well as the private company SpaceX have dedicated research to the question and evaluated several so-called "regions of interest" for their possible sustainability of human life. This includes considerations concerning available resources and local geography. The area for a human colony must enable the extraction and processing of local sub-surface ice deposits to generate water while

also featuring resources to produce in-situ propellant. Next to these requirements a maximum latitude of 40° North or South or as close as possible to the equator has been determined to address sun light intensity for utilising solar energy and thermal management considerations (LPI, NASA, 2021). Additionally, engineering constraints to provide a safe and secure descent and landing are important to consider. These constraints include a low elevation, with its corresponding high atmospheric density to enable aerobraking even for high-payload deliveries, preferable below 2 km with respect to the MOLA geoid. Landing a spacecraft requires an even, load bearing surface with a minimal slope angle and clearance of loose rocks that can potentially damage the craft during its descent. Therefore, a slope inclination of less than 5° over a length of 10m and the chance of an impact with a rock of 1m diameter of less than 5% has been deemed desirable. To carry out a controlled landing the surface needs to be radar reflective to allow measurements of the distance to the surface. Factoring in all these requirements and constraints several spots in or near the Arcadia Planitia as well as the Phlegra Montes region have been identified as possible landing spots for a manned mission to Mars.

2.3 Simulations

The simulation of an AWES requires the combination of an appropriate representation of the atmospheric conditions as well as a realistic description of the deployed AWES. In this thesis, the Martian Climate Database is used to gain insight on the atmospheric conditions on Mars. To simulate the kite system and the resulting trajectory the open-source code LAKSA is used. In this chapter, both tools are introduced including their applicability and limitations.

2.3.1 Martian Climate Database (MCD)

The Martian Climate Database (MCD) enables the data collection of several atmospheric parameters obtained from a planetary or general circulation model. An example of the structure of a GCM is shown in Figure 11.

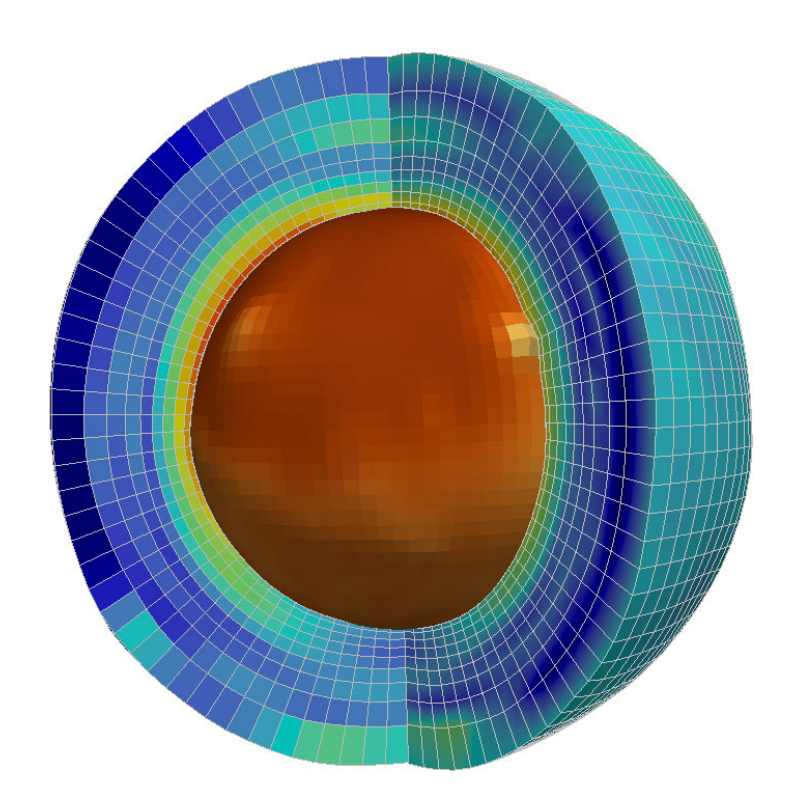


Figure 11: Grid structure of a GCM spanning the Martian surface and atmosphere Source: https://gem-mars.aeronomie.be

Before establishing a general circulation model (GCM) for the planet of Mars only the scarce data obtained by different missions like landers and orbiters was available. The first numerical simulations allowing a characterization of the atmosphere with a temporal and spatial coverage of Mars was first established in 1969 (Leovy and Mintz, 1969; Forget *et al.*, 1999). This first Martian GCM as well as later circulation model are generally comprised of two parts: the dynamics and the physics. The dynamics arise from the solution of the equations of meteorology based on the three-dimensional

Navier-Stokes equations. Since the dynamical core largely coincides for any planetary GCM, the dynamic core of the model of Earth can be adapted to resemble Mars by altering different parameters, such as the rotational rate, the specific gas constant, and the planet's radius (Lewis, 2003; Forget *et al.*, 1999).

The circulation models of the atmosphere are based on the equations of hydrodynamics and are integrated over space and time. These models have successfully reproduced observations confirming their potential usefulness for data collection and analysis. To address topics such as aerobraking, descent, landing, and more, GCMs offer a three-dimensional time-dependable atmospheric state, providing important data for planning of these phases of the mission (Forget *et al.*, 1999).

In 1995 a Mars-GCM, meanwhile named the PCM, was developed in a collaborative effort by the Laboratoire de Météorologie Dynamique (LMD) in Paris, the Atmospheric, Oceanic and Planetary Physics at Oxford University (AOPP) in Oxford with support of the European Space Agency (ESA), the Centre National de Recherche Scientifique (CNRS), and the U.K. Particle Physics and Astronomy Research Council assisting the ESA with future designs of missions, forming the basis of the Martian Climate Database or MCD (Lewis, 2003; Forget *et al.*, 1999).

The structure of the data base is based on an evenly spread grid with 64 x 49 (longitude x latitude) points spanning the surface of Mars. This corresponds to a latitudinal spacing of 3.75° and a longitudinal spacing of 5.625°. All available variables are stored in these grid point on 73 levels vertically, with the lower atmosphere reaching up to level 53. To obtain data between the grid points on or between different vertical levels, the variables are either interpolated linearly or bilinearly depending on the variable. Temporally, the data is structured around 12 Martian months, each corresponding to 30° solar longitude, each comprised of 46 to 66 sols resulting from the planets' eccentricity. The data is stored every two hours, with a Martian hour defined as 1/24th of a sol. The reference time is set to the local time at 0° longitude, the Mars Universal Time. Interpolating for a requested time of year and of day is done linearly or bilinearly between encompassing months and Martian hours (F. Forget, E. Millour, T. Pierron, M. Vals and V. Zakharov (LMD), and the MCD team; Forget *et al.*, 1999).

The database offers different climate scenarios concerning dust and extreme ultraviolet radiation (EUV), with the latter only impacting the upper atmosphere or thermosphere. Also included are the last the last Martian years of 24 till 34 roughly corresponding to the Earth years 1998 till 2017 respectively (Piqueux *et al.*, 2015). The "Climatology" scenarios are based on the combination of the available observations of several Martian years to model the atmosphere and its dust distribution, excluding years with GDS (F. Forget, E. Millour, T. Pierron, M. Vals and V. Zakharov (LMD), and the MCD team).

The MCD will be used to derive wind speeds and atmospheric density values for the simulation to mimic the atmospheric conditions on Mars at a given location. The next chapter is concerned with the AWE simulator, introducing the software and its parametrisation.

2.3.2 LAKSA

The Lagrangian Kite Simulator, short LAKSA, is a MATLAB based simulator that uses the Lagrangian formalism of the equations of motion to simulate a kite or drone in flight. To quote the authors themselves, it is a "Parallelized flight simulator for the dynamic analysis of airborne wind energy systems for ground and fly-generation configurations" (Sánchez-Arriaga et al., 2019). The code is open access (Gonzalo Sánchez-Arriaga and Alejandro Pastor-Rodríguez) with user inputs including the physical parameters, control laws and the conditions for the initialization resulting in a simulation tool that is "in a very good qualitative agreement with the experimental data" (Sánchez-Arriaga et al., 2019). The approach of the LAKSA as well as its mathematical formulation and validation of the code is described extensively in the sources (Sánchez-Arriaga et al., 2017; Sánchez-Arriaga et al., 2018; Sánchez-Arriaga et al., 2019; Alonso-Pardo and Sánchez-Arriaga, 2015) by the creators and authors.

The Langrangian formulation results in a mathematical model comprised of a set of ordinary differential equations free of algebraic constraints. The main advantage of the lagrangian formalism is its minimal-coordinate approach, with several variables not having to be explicitly defined. By using the mathematical model as a fundamental outline, different types of kite and operational modes are defined as cases of this model allowing for an easy adaptation of this modular approach. In this thesis the relevant case is the so called "KiteFlex" model, allowing the simulation of a ground generating system in combination with a flexible tether, hence the name. The specific case is discussed in (Sánchez-Arriaga *et al.*, 2019).

The simulated AWES is characterised by three parameters: The kite's mass M_K , the initial tether length L_{T0} , and the gravitational acceleration g. These are used to attain dimensionless variables as well as further parameters.

In previous works, the kite was often modelled as a point mass. While this definition offers a useful approximation to estimate certain values such as the average power output, an analysis of the kites' aerodynamic interactions such as lift and drag forces require a more refined and detailed model. For this reason, LAKSA uses a rigid body approach characterised as a compromise between sufficient accuracy of the kite's behaviour and efficient calculations with respect to time and computational resources. The corresponding frame of reference originates in the centre of mass.

Instead of a direct connection of kite and tether, LAKSA uses the bridle lines as a joint. Connected with the tether via point Q, these lines are described as massless straight rods, as they are light compared to the tether, and are always under high tension. This approach eliminates the necessity of further details such as the number of bridle lines or the exact location of the attachment points at the kite. The simplification also leads to the bridle lines acting as geometrical constraints with only the position of point Q and the centre of mass of the kite being relevant. Figure 12 depicts the different frames of references as well as the bridle line arrangement.

While the physical model of the kite as a rigid body yields a sufficiently precise description of its dynamic behaviour, the accurate simulation of the tether is more difficult. In earlier simulations the tether is mostly depicted as a straight tether. This simplification yields accurate results for power calculations, as it simulates the tether under tension. However, even when the tether is under tension, the tether sags due to the gravitational force of its mass as well as its non-negligible aerodynamic drag when in motion. The authors of LAKSA opted for simulating the tether as a set of stiff rods connected by "ideal rotational joints" with each other. This tether model as a chain of stiff, inelastic rods enables the simulation of the sagging of the tether while also eliminating certain tether oscillations resulting in a resource efficient computation. Including the sagging of the tether reveals a lower flight altitude compared to straight tether impacting the simulation results. the rods are modelled being infinitely thin with just two angles needed to define their orientation.

In general, the input parameters for the program are the initial conditions, the physical parameters and the implemented control laws. The output of the simulation includes the temporal history of the kite's position, its velocities and angles, the tether tension as well as more. With the comparison of the solution with the classic mechanics formulation of Newton's laws, the range of the calculated derivation allows for a comparison of the results (Sánchez-Arriaga *et al.*, 2019; Sánchez-Arriaga *et al.*, 2018).

The model of the kite is defined by its mass, the chord length c, its wingspan b, and its surface S. It is possible to adjust the height of the kite, although it is only relevant for plotting the kite. To incorporate its dynamic behaviour the moment of inertia of the kite with respect to x_B-, y_B-, z_B-coordinate and the xz_B-plane is also defined (Figure 12b). The simulator uses a simplified kite model with a semi-elliptical cross section and the centre of mass placed at the intersection of the two planes of symmetry (Alonso-Pardo and Sánchez-Arriaga, 2015).

The atmospheric conditions are represented by the atmospheric density and the prevailing wind speed. The implementation of the wind speed includes a dynamic, oscillating description as well as a logarithmic wind speed law based on a set reference height. The tether is characterised by its density ρ_T , its diameter D_T and connects the

generator, that is not simulated, with point Q (Figure 12a). The simulator allows for the choice of the number of rods to represent the tether and adjust its flexibility, which has a significant impact on the necessary computational resources. While increasing the number of rods approximates reality and increases accuracy, the simulated results do not significantly change when implementing four or more rods (Sánchez-Arriaga *et al.*, 2019).

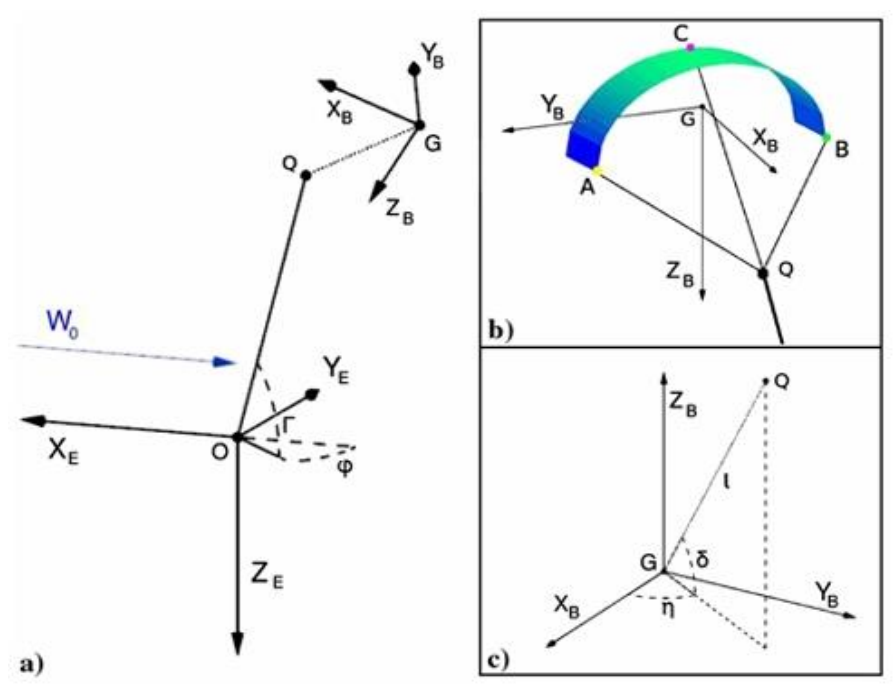


Figure 12: Frames of Reference used in LAKSA; (a) Body frame of reference of the kite with respect to the Earth Frame of Reference with wind speed W_0 ; (b) kite and arrangement of Bridle Lines; (c) orientation of bridle line with respect to the bridle length I, the bridle angles δ and η Source:[33]

The kite control functions implemented into the simulator result in a simplified dynamic model. It does not describe a self-consistent dynamical system and does not involve real-time inputs. The input parameters include the choice of the bridle length l_b , the vertical and horizontal angle, δ and η respectively, of point Q with respect to the kite's coordinate system, as shown in Figure 12c. Further, LAKSA allows to set the duration of the linear and circular section of the figure-of-eight trajectory. The characteristic non-dimensional time T_L for the linear section defines the duration the bridle line takes to turn from η to $-\eta$ and vice-versa. The non-dimensional circular time T_C defines the duration of the turning manoeuvre, in which the bridle line is deflected by the angle η or $-\eta$ with respect to the kites' body coordinate system.

The simulator includes a function to find periodic orbits suitable for power generation providing stable trajectories. However, the applicability is limited to the underlying mathematical nature of the solver, making it difficult to find such orbits at all (Borobia *et al.*, 2018). This leads to the uncertainty if a solution does not exist for the specified

combination of control variables, if it cannot be found based on the physical input, or it simply does not exist at all. Besides this periodic trajectory solver, an equilibrium function based on the acting forces on the kite, computes a stable position of the kite for the given wind speed and atmospheric density.

LAKSA offers an extended range of describing the dynamical nature of an AWES by including the flexibility of the tether as well as the aerodynamic behaviour of a rigid body. However, these extensions are also limited in their applicability. The tether description does not account for the tether's inertia, while the rigid body approach leads to an inadequate representation of soft wing designs. These kites are subject to deformation during flight and manoeuvres due to the flexible structure, altering their aerodynamic characteristics (Borobia *et al.*, 2018).

With the description of the utilised simulation tools for the atmospheric dynamics of Mars and the AWES simulator LAKSA, the following chapter is concerned with the approach of creating the simulation.

3 Methodology

In this chapter the approach used in this thesis to simulate an AWES in the atmospheric conditions of Mars with LAKSA is laid out. Considering a possible landing site for a manned mission, the method for data collecting of the local wind field, and the applied tools for analysis will be introduced. Furthermore, an appropriate kite system and mode of operation for the simulation will be chosen. Finally, the assumptions for a calculation of the potentially generated power are discussed.

Wind Field Evaluation

A promising landing site for a manned mission to Mars is the location near the Phlegra Montes at 35.23°N latitude and 163.95°E longitude. Satisfying the requirements and considerations for a possible outpost, it is one of the four primary sites selected by SpaceX in cooperation with several universities and NASA presented at the 2021 "52nd Lunar and Planetary Science Conference" (LPI, NASA, 2021). In Figure 13 the chosen landing sites are depicted, with Phlegra Montes being point PM-1 in the red circle.

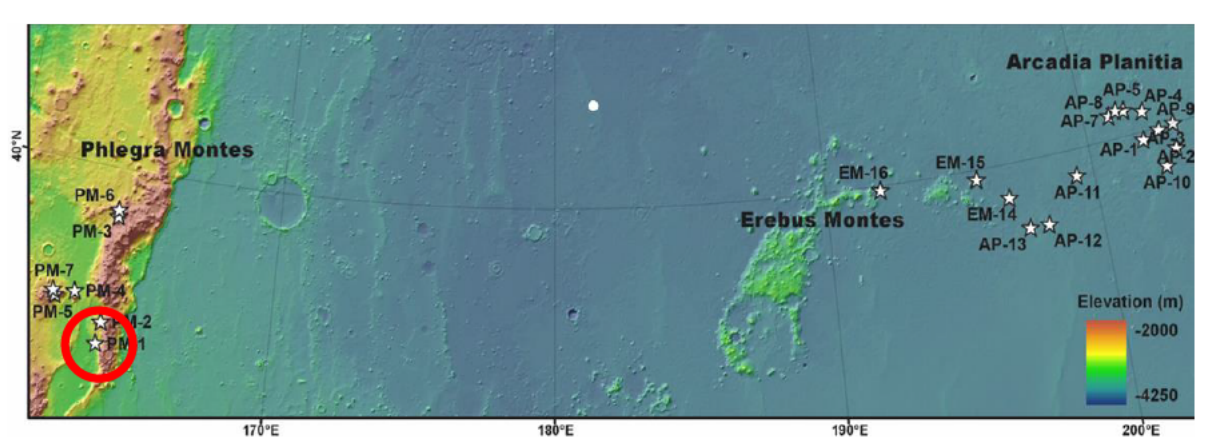


Figure 13: Marked locations as potential landing Spots for a manned Mars mission Source: [23]

Using the coordinates the necessary data can be extracted from the MCD. By plotting the horizontal wind speeds and atmospheric densities over 360° of solar longitude and all 24h of a sol, the diurnal and annual fluctuations are included.

As discussed in 2.3.1 the data of the MCD has some constraints and values are mostly interpolated. This leads to data with limited accuracy, especially concerning temporal constraints. Acquiring high resolution wind speed data thus enabling a realistic simulation of the prevalent wind speeds and their variations for any location on Mars at any time is therefore not possible. Since this work's goal is to present a simulation of a kite in the Martian atmosphere a total analysis of the fluctuations, probability of wind speeds at the site, and the wind speeds and densities during atmospheric phenomena will not be discussed. The presented data aims to give an insight of the

prevailing atmospheric conditions to enable a first attempt of the simulation of an AWES on Mars. Therefore, this thesis will only investigate the flight conditions given by the "clim ave" scenario, containing the averaged wind speed and density values over all observed Martian years 24 to 34. Since wind power is proportional to the wind speed cubed but only linearly to the density, the choice of the atmospheric conditions for the simulation depends on the wind speed. With the results of the data collection the settings for the AWES simulation are set.

Choice of AWES

For the simulation of an AWES on Mars, the choice of the kite structure and mode of operations need to be determined. Given the fact that weight is still a fundamental limit for any object brought to space, the system needs to exhibit a high energy density, meaning a low weight in respect to the generated power. Furthermore, space travel requires compactness and lightweight of the payload in order to fit as much equipment as possible in the bulk of the spacecraft. This leads to a soft wing design operating in a pumping cycle as a promising candidate allowing the kite to be folded, minimizing the necessary space aboard. The accompanying ground station needs to include the generator, the winch, as well as an energy storage system representing the bulk of the weight of the entire AWES. However, as a human colony necessitates a robust and redundant energy system, a storage facility is required anyway. Additionally, the simplicity of a parafoil lowers the complexity of the system enhancing the robustness and durability of the system in extreme conditions as observed on Mars. It also lowers the weight of the tether since electricity conduction does not need to be considered, allowing the use of lightweight high-tensile-strength fibres. If the operation of a rigid wing design is even possible is up for debate given the extreme low density of the atmosphere, to generate the necessary lift to overcome its weight.

Simulating AWES in LAKSA

With the choice of an AWES concept, the LAKSA input is adjusted to the environment to proceed with the simulation. As described in 2.2.2 using the scaling factors of Schmehl et al. the kite dimensions as well as its properties are adjusted. It is assumed that the aerodynamic coefficient of the kite does not change whether deployed on Mars or Earth based on the 2D considerations in (Gaunaa *et al.*, 2024) assuming an equal aspect ratio. The kite model used in the simulation is the "Cabrinha Contra", a surf kite, that has been tested for use as part of an experimental AWES (Borobia *et al.*, 2018). Since the scaling factors depend on the atmospheric conditions, the original and scaled values are presented after the wind field analysis results.

The LAKSA simulation aims to investigate if a stable flight in the atmosphere of Mars is possible using a scaled version of a kite tested in the atmosphere of our planet. The investigation and implementation of the optimal control inputs is out of the scope of this work. Therefore, neither the reel-out nor the reel-in phase is demonstrated, with

the successful demonstration of a stable figure-of-eight trajectory as the goal of this thesis. Assuming the ability to adjust the lift coefficient with the appropriate control inputs implies a possible reel-in and -out manoeuvre.

The scaled kite model and the physical parameters are then implemented in the LAKSA code. While the dimensions of the kite are directly derived from the scaling factors, the moment of inertia cannot simply be derived the same way. However, since the moment of inertia is calculated by multiplying the mass with the distance to the axis of rotation squared, a simple and conservative assumption by scaling all entries in the tensor of inertia by the scaling factors of the mass times the square of the largest one-dimensional scaling factor, the wingspan factor. Since one requirement of the scaling approach is based on the unchanged aspect ratio, the adjustment of the cord length is derived from dividing the newly attained planform area by the altered wingspan. While this approach is based on calculating the standard mean chord, it is assumed that every chord length of the kite is scaled by the same factor. Although the height parameter of the kite is only used for plotting purposes it will also be scaled by the same factor as the wingspan.

As already mentioned in chapter 2.3.2, with the limited gain in accuracy by increasing the number of rods representing the tether, the number is set to three. The settings for defining the numerical approximation are altered to accelerate the computational time. Mainly the tolerances for the numerical integration are increased as well as the number of time steps lowered. At this point, there will be no further explanation of the utilised code with the next chapter documenting and presenting the trial to achieve the simulation.

Power Calculation

The calculated power generation is based on the equations presented in chapter 2.1.2. Assuming the necessary variables based on the presented simulation and the Python script from (Schmehl), the power output is calculated. The utilised Python script as part of (Schmehl *et al.*, 2024) is design to specifically calculate the pumping cycle power of an AWES on Mars.

After estimating the power output, the results and a comparison with the energy requirements mentioned in 2.1.2 for a 500-sol, manned mission with a crew of six is discussed.

4 Results

In this chapter the resulting atmospheric conditions are presented as well as the simulation result using LAKSA, and finally the potential energy output under optimised conditions. After a short presentation of the prevailing atmospheric density and corresponding wind speed, the parameters used in the simulation are selected.

4.1 Wind Field Analysis

Before simulating the AWES at the most promising landing zone so far, the prevailing wind speeds in the expected height of the flight trajectory needs to be evaluated. While this does not include a thorough analysis of the atmospheric conditions and its causes, a short evaluation of the findings is given.

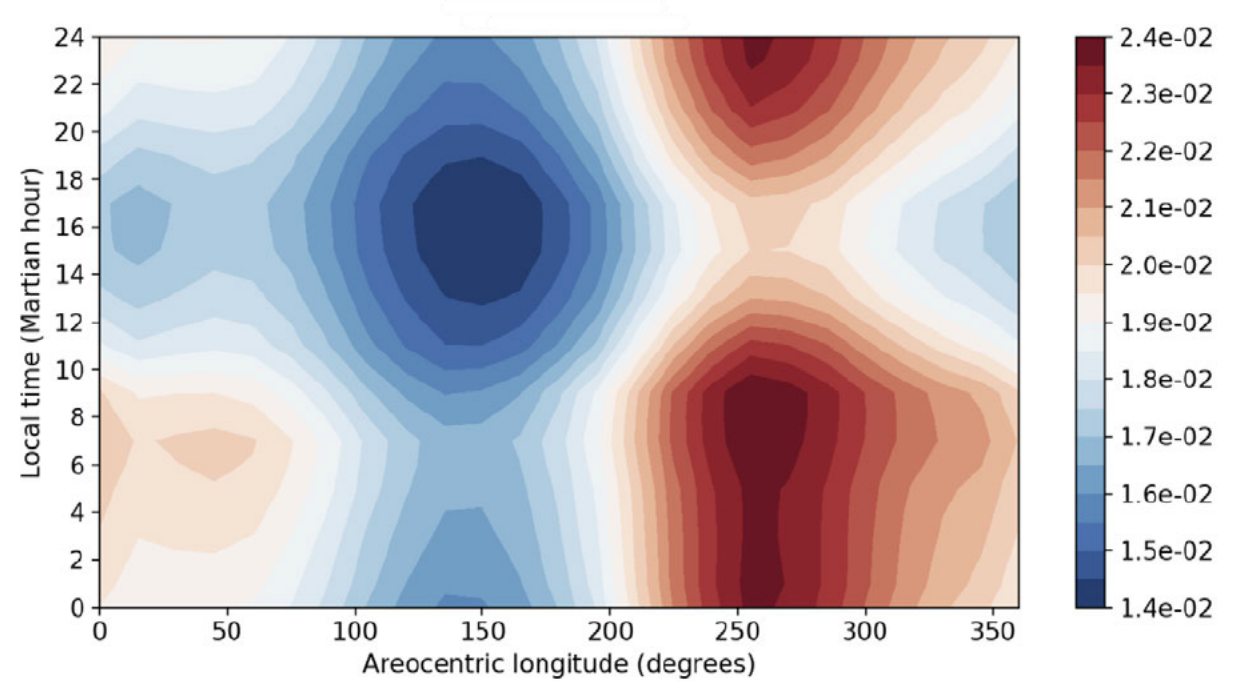


Figure 14: Atmospheric density at 35.23N 163.95E in 250m as simulated by the MCD

In Figure 14 and Figure 15 the daily density and wind speed at the landing site candidate PM-1 over a Martian year or 0 to 360° solar longitude at an altitude of 250m are depicted. Looking at the density distribution a seasonal variation is noticeable based on the colour scheme.

With the onset of winter in the northern hemisphere at around 180° solar longitude the density significantly increases leading to an especially dense atmosphere from around 220° to 320° SL. This increase coincides with the begin of the dust storm season in the northern hemisphere. Easily noticeable are the diurnal fluctuations during winter and summer showing the influence of solar radiation impacting the lower atmosphere. With the density being low during daytime, due to the warming of the atmosphere by

the sun, it increases again during night-time. The significant differences of day- and night-time duration over the year can be derived from the latitude of the landing site candidate at 35.23° North.

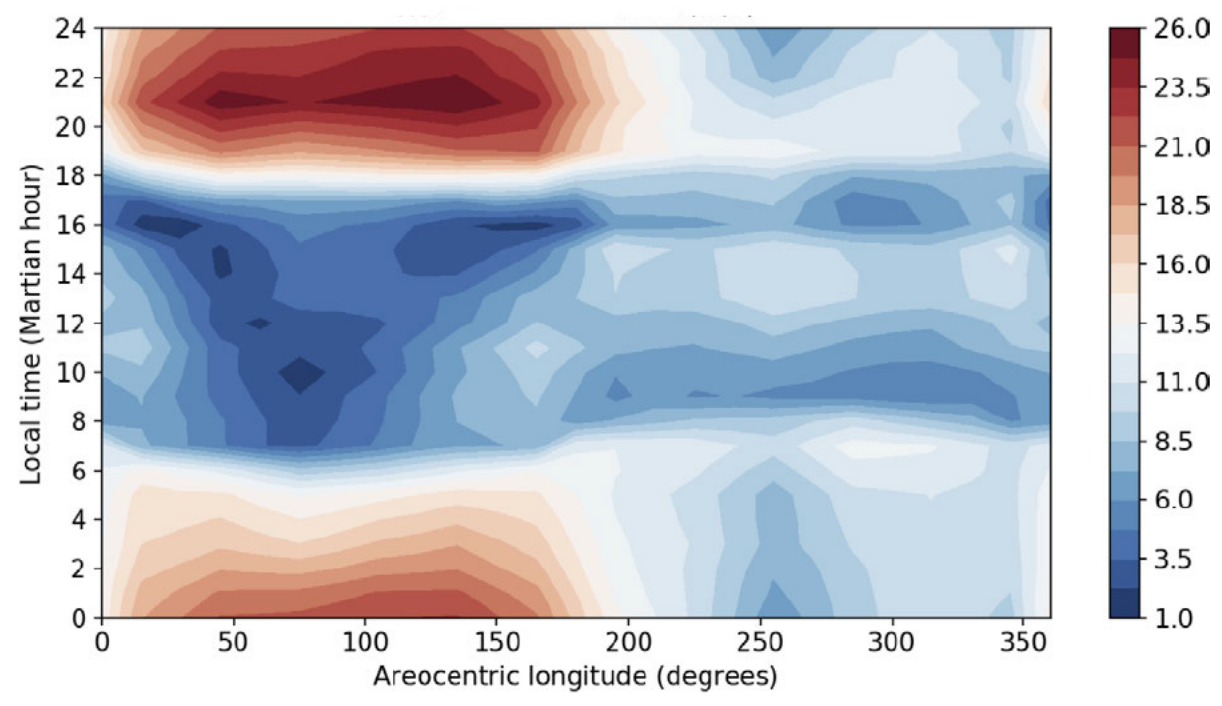


Figure 15: Horizontal wind speeds at 35.23N 163.95E in 250m as simulated by the MCD

Analysing the horizontal wind speed distribution reveals a prominent seasonal variation. While wind speeds seem to be on a low-level during day-time year-round with the begin of the northern summer season, the nighttime wind speeds increase significantly, reaching up to $26 \, \frac{m}{s}$. However, with the onset of the winter season in the northern hemisphere, the modelled wind speeds drop off. This also includes a lower diurnal fluctuation. As with the atmospheric density, the duration and intensity of the solar radiation has a significant impact, causing high diurnal atmospheric gradients during the summer and lower daily variation during winter times. While the climate scenario of choice does not include Martian years with GDS, the higher dust content in the atmosphere during northern winter could also influence the radiation intensity reaching the lower atmosphere. With most of the high wind speeds occurring roughly between Martian hour 18 to 6 and between solar longitude 0° to 180° , this time frame presents the highest potential for wind power generation.

To derive a possible use case from the attained atmospheric density and horizontal wind speeds in 250 m above the Martian surface at the landing site PM-1 the focus will lie on the wind speed distribution. For the simulation in the following chapter the wind conditions of nighttime roughly during 0° and 180° is used as input parameters. Utilising a general and conservative approach the wind speed will be set to $23^{\frac{m}{5}}$ and

the atmospheric density to 0.016 $\frac{kg}{m^3}$, representing almost optimal conditions for the landing site at Phlegra Montes. With the determination of a flight condition with respect to wind speed and atmospheric density, the LAKSA kite model is scaled, and the trajectory is studied.

4.2 LAKSA Simulation

In this chapter, the simulation results and subsequent adjustments to the control parameters to achieve a steady flight path for the Mars-kite in each scenario-case are presented. Before documenting the simulation results with the adjusted parameters for the Martian atmosphere, the simulation of the reference kite using the atmospheric parameters of Earth is shown utilising the full potential of LAKSA.

The adjustments of the kites' dimensions are based on the first case with a wind speed of $23\frac{m}{s}$ and an atmospheric density of $0.016\frac{kg}{m^3}$. This is based on the expected factors and their influence on the plan area of the kite. The bigger the area the bigger the lift generation, enabling it to potentially deal with significantly lower wind speeds. The reference parameters are set to $12\frac{m}{s}$ of wind speed and a density of 1.215 $\frac{kg}{m^3}$ corresponding to the atmospheric density on Earth in 250 meters according to the ISA. This results in the wind speed and density scaling factors (23) and (24).

$$K_{\rho} = \frac{0.016}{1.215} = 0.0132 \tag{23}$$

$$K_{vw} = \frac{23}{12} = 1.917 \tag{24}$$

With these factors the dimensions of the Mars kite are calculated using the equations given in 2.2.2 and are summarised in the Table 1.

Table 1: LAKSA kite parameters and scaling factors				
Param	neters	Scaling Factor	Original Value	Scaled Value
S	[<i>m</i> ²]	10.754	13	130.802
h	[m]	3 270	5	16 305

i ai	arriotoro	Obaining i dotor	Original Value	Coaloa Valao
S	[<i>m</i> ²]	10.754	13	130.802
b	[m]	3.279	5	16.395
Cmea	an [<i>m</i>]	3.280	1.5	4.920
m	[kg]	1.711	3.4	5.817
dt	[m]	0.722	0.002	0.00144
lx	$\left[\frac{kg}{m^2}\right]$	7.763	12.10	93.932
lγ	$\left[\frac{kg}{m^2}\right]$	7.763	3.2	24.842
lz	$\left[\frac{kg}{m^2}\right]$	7.763	11.4	88.498
I _{XZ}	$\left[\frac{kg}{m^2}\right]$	7.763	0.4	3.105

First, the reference flight trajectory of the Earth kite version is presented. Using the periodic orbit solver a solution is found for the input parameters of Table 2 using the

original kite dimensions. The length of the tether is set to 400m, and the resulting periodic orbit error is 0.037919.

Table 2: Control input of reference kite using Periodic orbit solver

lΒ	[m]	4
δ	[m]	70
η _{max}	[°]	12.5
TL	[°]	1.7
Tc	[-]	1.4

The simulated figure-of-eight is shown in Figure 16a. The height of the trajectory is low, exhibiting an average elevation angle of less than 20°. However, attempts to alter the position of the trajectory with respect to the Earth frame of references failed. Nonetheless, this example figure-of-eight showcases a potential flight path useful for power generation.

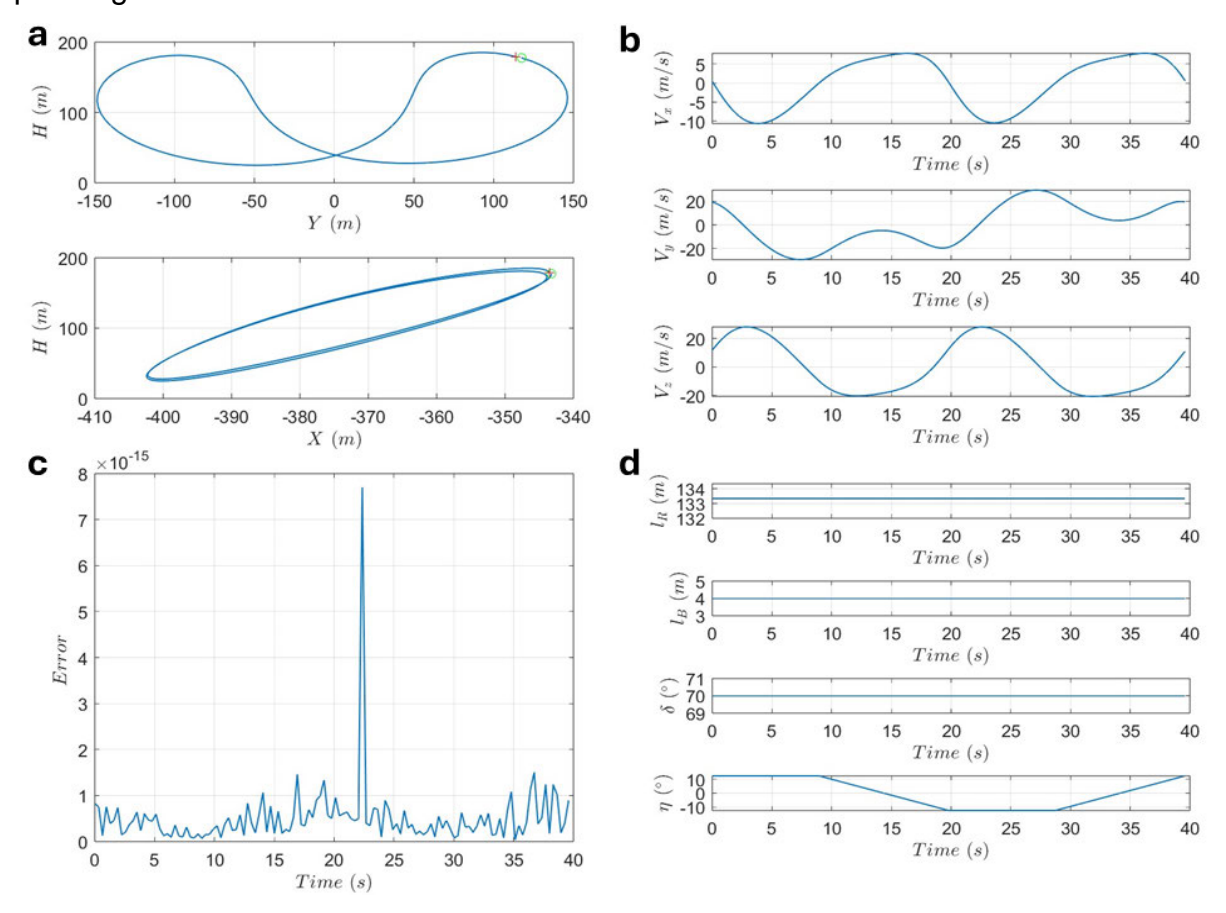


Figure 16: Simulation results of reference kite using the periodic orbit solver; (a) trajectory in XYZ-coordinate system; (b) velocities in their respective coordinate; (c) error with respect to classical mechanics; (d) top to bottom: length of tether rods, bridle line length, bridle angle δ , change of bridle line angle η during manoeuvre

The resulting tether forces during the manoeuvres reach a maximum of 1419.5 N. This correlates to the apparent kite speed shown in Figure 16b, that significantly exceeds the wind speed of $12 \frac{m}{s}$. The maximum kite speed of $29.091 \frac{m}{s}$ is reached at ~22.1 s The error with respect to the classic mechanical formulation, as depicted in Figure 16c stays within the order of 10^{-15} , only spiking once, presumably when the kite reaches its maximum velocity.

The periodic solver integrated in LAKSA is successfully applied to the reference Earthkite system. The same simulation input combined with a periodically varying wind speed led to viable solution, therefore the presented simulation was performed using a constant wind speed. The periodic orbit solver is also applied to the scaled Marsversion of the kite, although no results can be presented. After extensively varying the control inputs, the bridle length, the bridle angle δ , as well as the steering angle η , and the duration for each segment of the trajectory no solution was found. Every input combination resulted in a periodic orbit error far beyond one, either generating trajectories below the XY-plane representing the surface of Mars or not finding a numerical solution at all. While an increase and decrease of the periodic error with varying input could be observed these changes were deemed not suitable for drawing conclusion for the kite design or control. Since an equilibrium and a stable trajectory was found it is unclear whether a periodic orbit satisfying the solvers conditions exists or not. Since this problem also arises for altered input parameter using Earth specific values, not finding a periodic solution for the Martian environment cannot be counted as a meaningful result. Therefore, a comparable figure-of-eight flight-path for Mars as in Figure 16 is not presented. To avoid this numerical problem, the function to determine a periodic orbit is not used anymore. However, the same control law leading to an oscillating steering or lateral bridle angle is used. Further, the behaviour of the kite with respect to the control inputs is investigated.

For this reason, only the function to find an equilibrium is utilised in combination with limited control inputs. It is obvious that the presented trajectory in Figure 17a is far from ideal for use in the power production cycle of an AWES, however it clearly showcases the possibility of flight in the Martian atmosphere. The flight path was deemed stable as no significant change in altitude was observed over an extended time and the occurrence of consistent variability of the parameters describing the trajectory is depicted in Figure 18. Additionally, the error with respect to classical mechanics consistently stays within the order of 10⁻¹⁵ (Figure 17c).

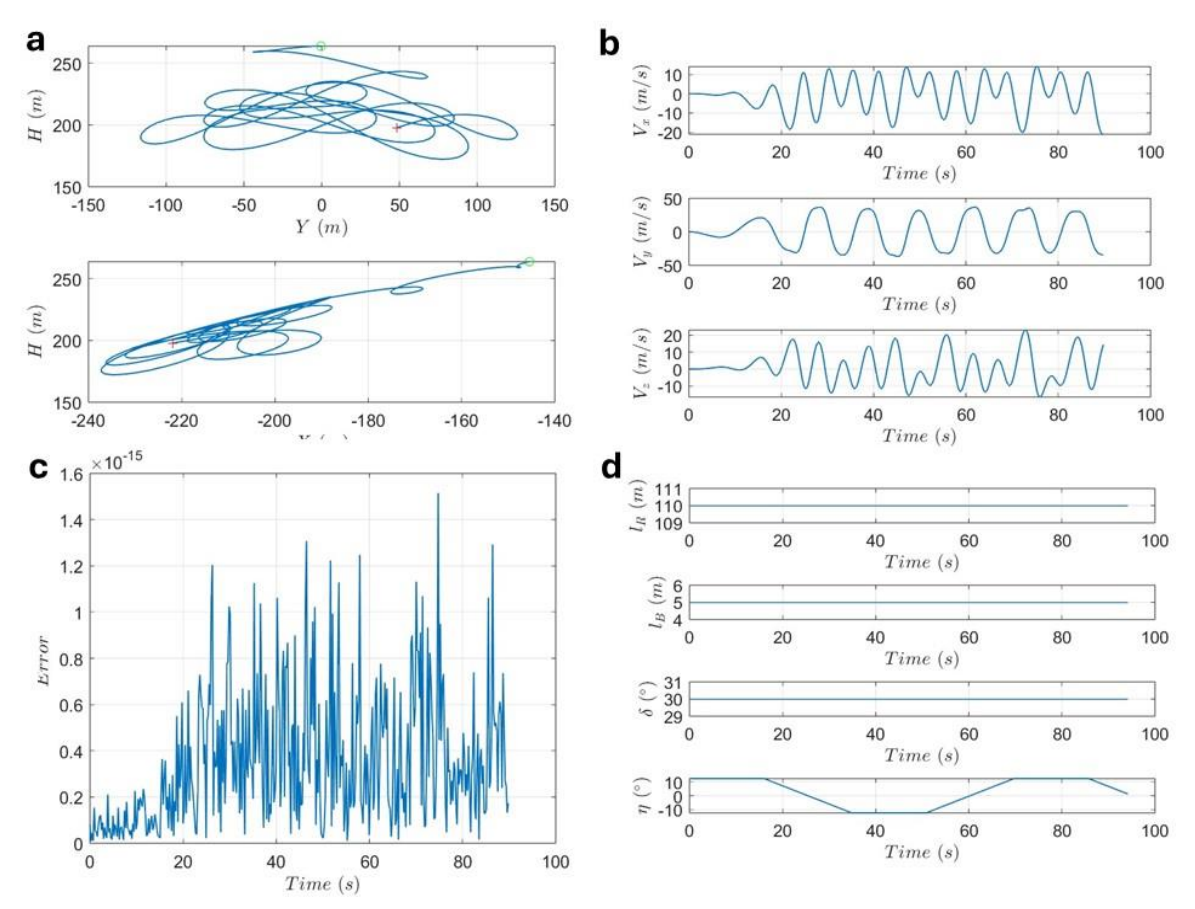


Figure 17: Simulation results of the scales Mars kite not using the periodic orbit solver; (a) trajectory in XYZ-coordinate system; (b) velocities in their respective coordinate; (c) error with respect to classical mechanics; (d) top to bottom: length of tether rods, bridle line length, bridle angle δ , change of bridle line angle η during manoeuvre

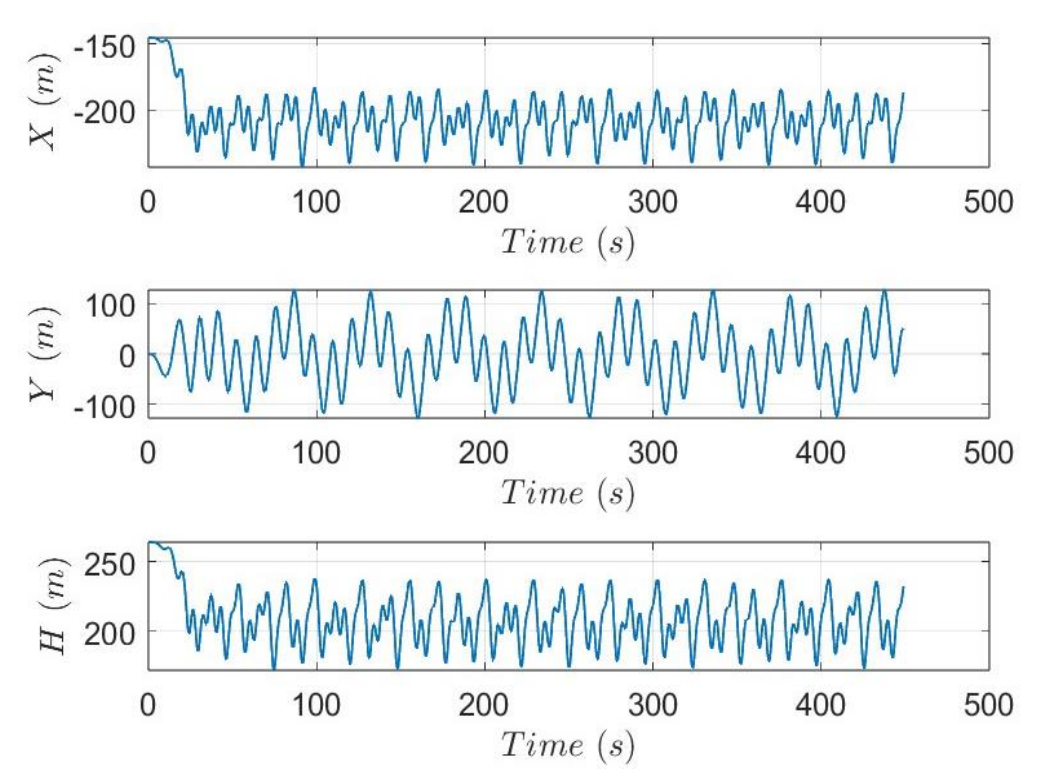


Figure 18: long term behaviour of Mars kite with periodic fluctuations

Beginning with the control parameters used for the periodic solution of the Earth's kite, the search for applicable values for the Mars kite not resulting in an unstable or impossible flightpath led to several changes with some tendencies being observed. For the given wind condition the trial-and-error approach to find viable control parameters (Table 3 and Figure 17d) resulted in a significantly reduced δ , from 60° to 30°. Further, the solutions became more stable with a higher ratio of T_L to T_C , which contradicts the expected increase in turning radius. With K_R = 3.675 the time necessary to perform the turning manoeuvre is estimated to scale proportionally, however the turning duration was lowered. Even with a relative low T_C the lateral bridle angle η was decreased.

Table 3: Control input of the scaled Mars kite

LT	[m]	300
lΒ	[m]	2.5
δ	[°]	10
$ \eta_{\text{max}} $	[°]	-7.5
TL	[-]	1.7
Tc	[-]	1.1

With significantly lower tether forces than the presented orbital solver simulation, the results hint at the differences the orbital solver makes. Comparing the simulated tether forces of the reference kite with the scaled Mars version, the force should scale by K_F = 0.522 accordingly. However, as depicted in Figure 19 the maximum tether force of the Martian kite only reaches ~320N, resulting in an observed tether force factor of 0.225 (Figure 19).

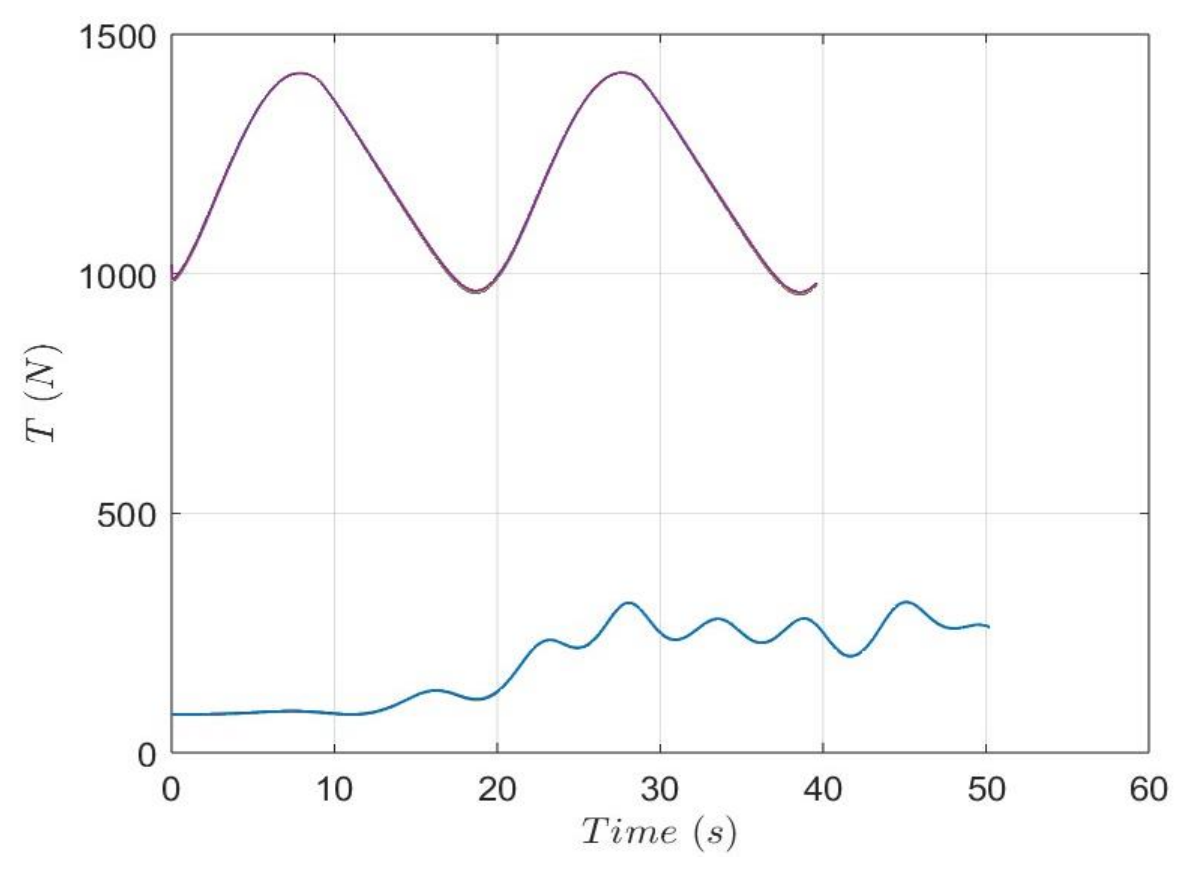


Figure 19: simulated tether forces of the reference kite (purple) and the scaled Mars kite (blue)

Notably, when comparing the angles of attack and side slip angles of the kite, the periodical orbit solution does not exhibit any side slip angle. Further, the non-periodically solved simulation does not reach the same angles of attack, lowering its lift coefficient and the aerodynamic efficiency.

While the kite reaches a maximum velocity of $\sim 43\frac{m}{s}$ at approximately 45 seconds (Figure 17b), the coinciding side slip angle β also reaches its maximum (Figure 20). This leads to the assumption, that the maximum velocity of the kite is not its apparent velocity v_a .

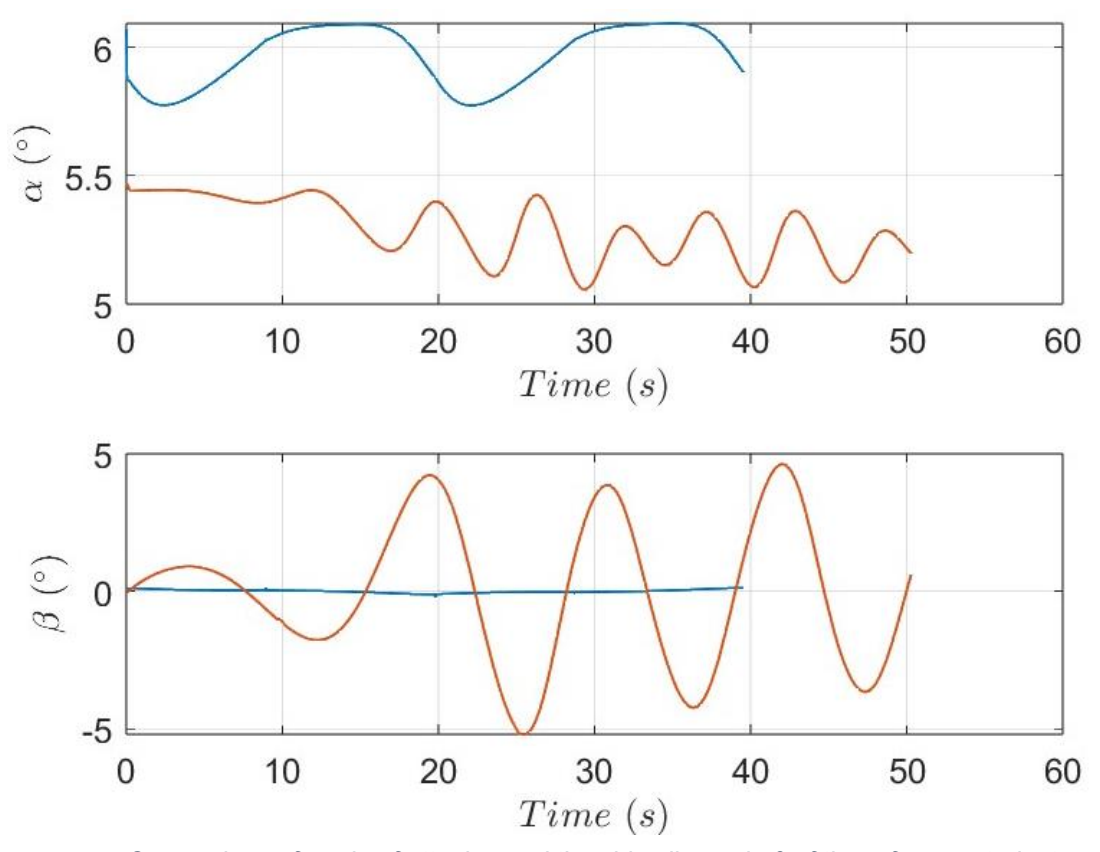


Figure 20: Comparison of angle of attack α and the side slip angle β of the reference trajectory utilising the periodic orbit solver (blue) and the Mars kite trajectory without the periodic orbit solver (orange)

In the next subchapter the energy output will be computed. With the figures in this chapter, the simulation of the Mars kite is not useful for the calcualtion. With a far lower tether force than the scaling factor K_F suggests as well as the considerable side slip angle, a python script by Schmehl et al. is used (Schmehl), assuming optimised values for the input parameters. The Python code is publically available and was created to analyse AWESs on Mars using the scaling method as done in this thesis. Therefore, some of the default values are used instead of using the the corresponding values resulting from the simulation above.

4.3 Theoretical Power Output

Before determining the power output, it is important to mention that the calculation of the power generation of the simulated kite and its resulting operational parameters was deemed not practical. However, to gain an understanding of the variables and influences affecting the system, the computation of the theoretical power output under almost optimal conditions is conducted.

To calculate the theoretical power output of the scaled kite on Mars, some assumptions and simplifications are made. Since the determination of the lift and drag coefficient in LAKSA is complex and dependent on six variables, the two necessary lift coefficients for the calculation of the power output are set to $C_{\text{L,out}} = 0.71$ and $C_{\text{L,in}} = 0.39$ as well as the drag coefficients $C_{\text{D,out}} = 0.14$ and $C_{\text{D,in}} = 0.39$. These values are derived from the default values of the publicly available script especially designed to calculate the power output of an AWES deployed on Mars (Schmehl *et al.*, 2024) with the drag coefficients being specific to the kite. This means, that the tether drag of $C_{\text{D.tether}} = 1$ needs to be included. The average elevation of the reel-out phase is set to match the angle of the simulations in 4.2 to approximately $\beta_0 = 43^\circ$. Using $z_m = 250$ m and considering the simulated trajectory as the beginning of the reel-out phase with $r_{min} = 300$ m, the rounded resulting maximum deployed tether length using equation (6) equals $r_{max} = 1000$ m.

Table 4: Input parameters for power calculation

Input Parameters		Input Values
ρ	$\left[\frac{kg}{m^3}\right]$	0.016
Vw	$\left[\frac{m}{s}\right]$	23
Α	[m ²]	130.802
C _{L,out}	[-]	0.71
$C_{L,in}$	[-]	0.39
C _{D,out}	[-]	0.14
$C_{D,in}$	[-]	0.39
$C_{\underline{D,tether}}$	[-]	1.0
r _{min}	[m]	300
r _{max}	[m]	1000

With these input parameters, the resulting reeling factors and tether forces are computed. The python script uses several functions to find optimised values resulting in f_{out} = 0.184 and f_{in} = -0.913.

The reel-out speed is set to the optimum of one third of the wind speed and the maximum reel-in speed set to -21 $\frac{m}{s}$ based on the default values of the script and the

assumed equal mechanical abilities of the system independent of the location of deployment.

The exhibited WPD is calculated to be $97.336 \, \frac{W}{m^2}$. Calculating the power output during reel-out and the power consumption during reel-in, the net output reaches approximately 8891 W at $23 \, \frac{m}{s}$ and an atmospheric density of $0.016 \, \frac{kg}{m^3}$. This value correlates with the tether force $T_{out}=3134$ N, exceeding the reference kite tether force by a factor of more than two.

As already mentioned in 2.2.2, a six-headed crew requires at least 576 kWh per sol for a 500-sol mission to Mars. Dividing the power requirement by the approximately 25 Martian hours of a sol, the necessary power output a 23.04 kW is derived. This leads to at least three AWES units to satisfy the requirement in high wind power density settings. Since most of the year exhibits far lower wind speeds albeit with a higher density, this is deemed to not be sufficient.

5 Discussion

While publications have deemed the deployment of an AWES in the Martian atmosphere feasible, this thesis attempted to simulate the flight trajectory of an airborne kite system. The trajectory was then compared to an optimised flight path utilising a periodic orbit solver. Since the simulation of the scaled Mars kite is not optimal and does not reflect a possible flight trajectory for a power cycle, only a few parameters have been further used to calculate the power output of the system. While a demonstration of a successfully completed flight trajectory of a pumping cycle is not presented, this attempt highlights several important considerations necessary to successfully and accurately simulate an AWES in the atmosphere of Mars.

Beginning with an assessment of the data used in this thesis the amount of data points used is insufficient. Since this thesis aimed to demonstrate a simulation in the Martian atmosphere it was deemed adequate, but in future a more thorough analysis of the local atmosphere with respect to altitude and time is necessary. In general, only considering wind speeds and densities does not give the whole picture. With tools like the MCD the available data are limited by its spatial and temporal grid spacing, resulting in estimated values without factoring in small scale influences such as local phenomena or topography. Furthermore, to adjust for variables ranging from the atmospheric viscosity, over perturbations caused by gravitational waves, to local Martian phenomena such as dust devils or cyclones requires live data and further experimental research on their influence on the atmospheric parameters. While the analysis given above is sufficient to determine a likely combination of wind speed and density for an AWES to be deployed, it does not allow for any further conclusion about the feasibility and reliability of such a system in this environment. Further analysis and testing are necessary to determine the take-off capabilities and minimum wind speeds for operations throughout the day and year. A complete analysis requires more temporal data points and an investigation of the variability with respect to the altitude. Furthermore, the influences of the local topography and air circulation patterns including vertical wind components needs to be studied.

The characterisation of aerodynamic behaviour in a given atmosphere requires rigorous experimental testing and the development of an appropriate kite design. The low density significantly alters the aerodynamics of any aircrafts compared to Earth's atmosphere influencing flow separation. This requires wind tunnel testing and simulations concerned with computational fluid dynamics in the appropriate conditions. Further, the structural behaviour of the kite in this environment involving its deformation and variable dimensions depending on the manoeuvre needs to be addressed. The design and conceptualisation of the helicopter and first flying vehicle on Mars, Ingenuity, showcases a successful example how to approach the specific challenges the Martian atmosphere poses.

Another source of error next to the data acquisition is the implementation of the gathered data. No simulator can implement a complete model of an atmosphere with all dynamic variabilities. The LAKSA input parameters to describe the atmosphere is limited to the wind speed and density leaving room for errors and no insight into specific behaviours of the kite in a dynamic environment such as a turbulent wind field. As already mentioned in 2.3.2 LAKSA offers advantages with respect to earlier simulators. However, the code and the numerical approach could not be suitable for the research question of this thesis. Even though the periodic orbit solver allows for simulating stable trajectories fit for power generation, a solution is not easily found, with little chance of analysing and interpreting the reasons.

Calculating the power output of the given AWES was severely limited by the simulation results and relies on several simplifications and assumptions. Therefore, the calculated results represent an optimised pumping cycle energy output. Further, the used atmospheric parameters are only present in Martian summer nights, resulting in a far lower power output for other seasons and daytimes.

Therefore, a decisive statement about the viability of an AWES for power generation is not possible except for the probable necessity of several units to be deployed to satisfy the power requirements of a manned mission. While only one energy storage enables the simultaneous operation of more than one system, each kite needs a generator as well as a winch. This necessitates a further analysis of the total mass the combined systems would exhibit potentially lowering the specific energy density and thus their advantage over other wind energy extraction methods.

6 Conclusion

This work was conceptualised to create and present a well-documented simulation of a soft wing kite AWES deployed in the atmosphere of Mars. Aiming to validate and demonstrate the use of AWESs as a feasible option to support the energy needs of a possible colony on Mars, data from the Martian Climate Database was integrated into the publicly available LAKSA to simulate the model and determine its power output.

With only a limited utilisation of LAKSA possible as no periodic orbit was attainable, the presented simulation results are not useful for a complete and precise analysis of the kite's trajectory in the given environment. By using typical values for the characteristics of soft kites and optimised values the power output calculation revealed an insufficient power generation to support a manned mission with a crew of six. Since the calculation were done based on simplifications and assumptions it does not allow for any further interpretation. Other simulators that are not specialised on kite control like LAKSA could yield better results. KiteSim for example simulates a complete cycle and calculates the cycle power, although the implementation of the atmospheric conditions is limited, and it does not include the planetary dependent gravitational acceleration.

Further research concerning the simulation of an AWES on Mars should focus on an adequate description and model of the atmosphere, a realistic simulation of a complete power cycle with the ability to implement the atmospheric dynamics as well as the real specific power density of such a system. Furthermore, the aerodynamics of a soft kite in a low Reynolds and Mach number environment the influence on the manoeuvrability needs to be investigated.

As the commercialization of AWESs progresses on Earth more and more flight data will be available, enabling improved kite designs and control laws. With present and future Mars missions continuously collecting atmospheric and topographic data, the GCM of the Red Planet will become more and more accurate.

7 References

- A. Spiga (LMD) and Web interface updated by T. Pierron (LMD) and A. Bierjon (LMD), "Mars Climate Database v6.1 The Web Interface. Open source python interface by", available at: https://www-mars.lmd.jussieu.fr/mcd_python/.
- Almatroushi, H., AlMazmi, H., AlMheiri, N., AlShamsi, M., AlTunaiji, E., Badri, K., Lillis, R.J., Lootah, F., Yousuf, M., Amiri, S., Brain, D.A., Chaffin, M., Deighan, J., Edwards, C.S., Forget, F., Smith, M.D., Wolff, M.J., Christensen, P.R., England, S., Fillingim, M., Holsclaw, G.M., Jain, S., Jones, A.R., Osterloo, M., Jakosky, B.M., Luhmann, J.G. and Young, R.M.B. (2021), "Emirates Mars Mission Characterization of Mars Atmosphere Dynamics and Processes", *Space Science Reviews*, Vol. 217 No. 8.
- Alonso-Pardo, J. and Sánchez-Arriaga, G. (2015), "Kite Model with Bridle Control for Wind-Power Generation", *Journal of Aircraft*, Vol. 52 No. 3, pp. 917–923.
- Bechtle, P., Schelbergen, M., Schmehl, R., Zillmann, U. and Watson, S. (2019), "Airborne wind energy resource analysis", *Renewable Energy*, Vol. 141, pp. 1103–1116.
- Borobia, R., Sanchez-Arriaga, G., Serino, A. and Schmehl, R. (2018), "Flight-Path Reconstruction and Flight Test of Four-Line Power Kites", *Journal of Guidance, Control, and Dynamics*, Vol. 41 No. 12, pp. 2604–2614.
- Cherubini, A., Papini, A., Vertechy, R. and Fontana, M. (2015), "Airborne Wind Energy Systems: A review of the technologies", *Renewable and Sustainable Energy Reviews*, Vol. 51, pp. 1461–1476.
- Diehl, M., Schmehl, R. and Ahrens, U. (Eds.) (2013), *Airborne Wind Energy, SpringerLink Bücher*, Springer, Berlin, Heidelberg.
- ESA, CNES, LMD, LATMOS, IAA, The Open University and University of Oxford (2006), "Martian Seasons and Solar Longitude. Martian Solar Longitude Ls", available at: https://www-mars.lmd.jussieu.fr/mars/time/solar_longitude.html.
- F. Forget, E. Millour, T. Pierron, M. Vals and V. Zakharov (LMD), and the MCD team, "Mars Climate Database Version 6.1. Detailed Design Document", ESA Contract No. .4000128572/19/NL/AS.

- Forget, F., Hourdin, F., Fournier, R., Hourdin, C., Talagrand, O., Collins, M., Lewis, S.R., Read, P.L. and Huot, J.-P. (1999), "Improved general circulation models of the Martian atmosphere from the surface to above 80 km", *Journal of Geophysical Research: Planets*, Vol. 104 E10, pp. 24155–24175.
- Gaunaa, M., Rodriguez, M., Ouroumova, L. and Schmehl, R. (2024), "Scaling Airborne Wind Energy Systems for Deployment on Mars", in Cervone, A., Bier, H. and Makaya, A. (Eds.), *Adaptive On- and Off-Earth Environments*, *Springer Series in Adaptive Environments*, Springer International Publishing, Cham, pp. 111–144.
- Gonzalo Sánchez-Arriaga and Alejandro Pastor-Rodríguez, "LAgrangian Kite SimulAtors (LAKSA)", available at: https://github.com/apastor3/laksa.
- Hartwick, V.L., Toon, O.B., Lundquist, J.K., Pierpaoli, O.A. and Kahre, M.A. (2023), "Assessment of wind energy resource potential for future human missions to Mars", *Nature Astronomy*, Vol. 7 No. 3, pp. 298–308.
- Jochem Weber, Melinda Marquis, Aubryn Cooperman, Caroline Draxl, Rob Hammond, Jason Jonkman, Alexsandra Lemke, Anthony Lopez, Rafael Mudafort, Mike Optis, Owen Roberts, Matt Shields (2021), *Airborne Wind Energy*, Golden, CO.
- Khan, Z. and Rehan, M. (2016), "Harnessing Airborne Wind Energy: Prospects and Challenges", *Journal of Control, Automation and Electrical Systems*, Vol. 27 No. 6, pp. 728–740.
- Leovy, C. and Mintz, Y. (1969), "Numerical Simulation of the Atmospheric Circulation and Climate of Mars", *Journal of the Atmospheric Sciences*, Vol. 26 No. 6, pp. 1167–1190.
- Lewis, S.R. (2003), "Modelling the Martian Atmosphere", *Astronomy and Geophysics*, Vol. 44 No. 4, 4.06-4.14.
- Loyd, M.L. (1980), "Crosswind kite power (for large-scale wind power production)", *Journal of Energy*, Vol. 4 No. 3, pp. 106–111.
- Martínez, G.M., Newman, C.N., Vicente-Retortillo, A. de, Fischer, E., Renno, N.O., Richardson, M.I., Fairén, A.G., Genzer, M., Guzewich, S.D., Haberle, R.M., Harri, A.-M., Kemppinen, O., Lemmon, M.T., Smith, M.D., de la Torre-Juárez, M. and Vasavada, A.R. (2017), "The Modern Near-Surface Martian Climate: A Review of In-situ Meteorological Data from Viking to Curiosity", *Space Science Reviews*, Vol. 212 1-2, pp. 295–338.

- Ockels, W.J. (2001), "Laddermill, a novel concept to exploit the energy in the airspace", *Aircraft Design*, Vol. 4 2-3, pp. 81–97.
- Ouroumova, L., Witte, D., Klootwijk, B., Terwindt, E., van Marion, F., Mordasov, D., Corte Vargas, F., Heidweiller, S., Géczi, M., Kempers, M. and Schmehl, R. (2021), "Combined Airborne Wind and Photovoltaic Energy System for Martian Habitats", 71-86 Pages / SPOOL, Vol. 8 No. 2: Cyber-physical Architecture #4.
- Peng, S., Yang, Q., Shupe, M.D., Xi, X., Han, B., Chen, D., Dahlke, S. and Liu, C. (2023), "The characteristics of atmospheric boundary layer height over the Arctic Ocean during MOSAiC", *Atmospheric Chemistry and Physics*, Vol. 23 No. 15, pp. 8683–8703.
- Perković, L., Silva, P., Ban, M., Kranjčević, N. and Duić, N. (2013), "Harvesting high altitude wind energy for power production: The concept based on Magnus' effect", *Applied Energy*, Vol. 101, pp. 151–160.
- Piqueux, S., Byrne, S., Kieffer, H.H., Titus, T.N. and Hansen, C.J. (2015), "Enumeration of Mars years and seasons since the beginning of telescopic exploration", *Icarus*, Vol. 251, pp. 332–338.
- Salma, V., Friedl, F. and Schmehl, R. (2020), "Improving reliability and safety of airborne wind energy systems", *Wind Energy*, Vol. 23 No. 2, pp. 340–356.
- Sánchez-Arriaga, G., García-Villalba, M. and Schmehl, R. (2017), "Modeling and dynamics of a two-line kite", *Applied Mathematical Modelling*, Vol. 47, pp. 473–486.
- Sánchez-Arriaga, G., Pastor-Rodríguez, A., Borobia-Moreno, R. and Schmehl, R. (2018), "A constraint-free flight simulator package for airborne wind energy systems", *Journal of Physics: Conference Series*, Vol. 1037, p. 62018.
- Sánchez-Arriaga, G., Pastor-Rodríguez, A., Sanjurjo-Rivo, M. and Schmehl, R. (2019), "A lagrangian flight simulator for airborne wind energy systems", *Applied Mathematical Modelling*, Vol. 69, pp. 665–684.
- Sánchez-Lavega, A., Del Río-Gaztelurrutia, T., Spiga, A., Hernández-Bernal, J., Larsen, E., Tirsch, D., Cardesin-Moinelo, A. and Machado, P. (2024), *Dynamical Phenomena in the Martian Atmosphere Through Mars Express Imaging*, Vol. 220.
- Schmehl, R., "Airborne Wind Energy On Mars", available at: https://github.com/awegroup/awe_on_mars.

- Schmehl, R., Rodriguez, M., Ouroumova, L. and Gaunaa, M. (2024), "Airborne Wind Energy for Martian Habitats", in Cervone, A., Bier, H. and Makaya, A. (Eds.), *Adaptive On- and Off-Earth Environments*, *Springer Series in Adaptive Environments*, Springer International Publishing, Cham, pp. 145–197.
- Schorbach, V. and Weiland, T. (2022), "Wind as a back-up energy source for mars missions", *Acta Astronautica*, Vol. 191, pp. 472–478.
- SMD Content Editors (2024), "Mars", available at: https://science.nasa.gov/mars.
- (2021), SpaceX Starship Landing Sites on Mars: Summary.
- Watson, S., Moro, A., Reis, V., Baniotopoulos, C., Barth, S., Bartoli, G., Bauer, F., Boelman, E., Bosse, D., Cherubini, A., Croce, A., Fagiano, L., Fontana, M., Gambier, A., Gkoumas, K., Golightly, C., Latour, M.I., Jamieson, P., Kaldellis, J., Macdonald, A., Murphy, J., Muskulus, M., Petrini, F., Pigolotti, L., Rasmussen, F., Schild, P., Schmehl, R., Stavridou, N., Tande, J., Taylor, N., Telsnig, T. and Wiser, R. (2019), "Future emerging technologies in the wind power sector: A European perspective", Renewable and Sustainable Energy Reviews, Vol. 113, p. 109270.
- Zhao, P., Li, R., Wu, P., Liu, H., Gao, X. and Deng, Z. (2023), "Review of Key Technologies of Rotary-Wing Mars UAVs for Mars Exploration", *Inventions*, Vol. 8 No. 6, p. 151.